Elsevier Editorial System(tm) for
International Journal of Hydrogen Energy
Manuscript Draft

Manuscript Number: HE-D-19-06183R1

Title: Deposition of Nanostructured LSM Perovskite Thin Film on Dense YSZ Substrate by Airbrushed Solution Combustion (ASC) for Application in SOFC Cathodes

Article Type: Full Length Article

Section/Category: Fuel Cells & Applications

Keywords: LSM perovskite; nanostructured cathode; SOFC; oxygen reduction reaction; airbrushed solution combustion (ASC).

Corresponding Author: Dr. Diego Pereira Tarragó, Ph.D.

Corresponding Author's Institution:

First Author: Diego Pereira Tarragó, Ph.D.

Order of Authors: Diego Pereira Tarragó, Ph.D.; Berta Moreno, Ph.D; Eva Chinarro, Ph.D; Célia F Malfatti, Ph.D; Vânia C Sousa, Ph.D

Abstract: To make SOFC high efficiency energy generation devices, thin ceramic films are proposed as their main components. The rate of the oxygen reduction reaction is relevant for the overall performance of the SOFC, hence a lot of attention is given to the cathodes and their interfaces. The airbrushed solution combustion (ASC) method was used to fabricate an LSM thin film on a dense YSZ substrate. A single phase LSM perovskite was obtained with very thin and interconnected porosity, and a small average grain size (55 nm). The nanostructured LSM thin film electrode showed a low total activation energy (1.27 eV) at high temperatures, but a high area specific resistance at 850°C (55 Ω.cm²). The activation energy for the dissociative adsorption and diffusion of oxygen was significantly low (1.27eV), while the charge transfer and oxygen ion migration activation energy at the LSM/YSZ interface (1.28 eV) was closer to those usually reported.

International Journal of Hydrogen Energy February 2nd, 2020.

Dear editor,

We appreciate your comments on our work and the chance to submit the revised version of our paper. Also, we are thankful to bring us the reviewer's comments, which helped us to make our paper better.

As you asked, we have improved the literature survey with papers from different journals. We would like to emphasize that, from our view, the high ASR values found in our research does not necessarily compromises the other results (activation energies and microstructural features), because we were able to separate the correlations between these properties and the microstructural and interfacial characteristics, as you may see in the revised version. Besides, this is the first research paper concerning the use Airbrushed Solution Combustion method and we believe that the IJHE is the perfect journal for this publication, because it was developed aiming the fabrication of fuel cell electrodes.

We kindly ask you consider the publishing of our revised paper and we are very thankful for the opportunity to publish this work in such prestigious journal.

Thank you.

Diego Pereira Tarragó, PhD.

Programa de Pós-Graduação em Engenharia de Minas, Metalúrgica e de Materiais – UFRGS - Av. Bento Gonçalves 9500 - Setor 4 - Prédio 74 - Sala 211 - CEP 91501-970 Porto Alegre RS, - Fone 51 3308-9475 Fax 51 3308-9469
http://www.ufrgs.br/ ppgem

*Suggested Reviewers

International Journal of Hydrogen Energy November 28th, 2019.

SUGGESTED REVIEWERS

1. Florence Ansart - ansart@chimie.ups-tlse.fr - Université Toulouse III Paul Sabatier

2. Glenn C. Mather - mather@icv.csic.es - Instituto de Cerámica y Vidrio

3. Fabio Coral Fonseca - fcfonseca@ipen.br - Instituto de Pesquisas Energéticas e Nucleares

REVISOR #1

- “First, the reported cathode performances are not advantageous as compared with traditional ones.”

“The correlation between the method and the microscopic structure of the cathode is not well established.”

R: You are correct, the resultant electrode ASR is higher than those found in the literature. That is what we stated in the paper, as you may see. On the other hand, we believe that the results of activation energies and approach given in the discussion, together with the use a novel deposition method, are worth of publishing. In the revised paper, we made an effort to deepen the arguing in the correlation between microstructure and electrochemical properties by adding more recent literature in the interpretation of the results.

- ‘The characterizations are too rough, and clear presentation is lacking.”

R: The description of the experimental procedure, section 2.2, was modified in the revised version and a scheme of the half-cell testing was added.

REVISOR #2

- “The cross-section SEM images of as-prepared cathode and surface SEM images of the measured one should be presented in the paper so that we can evaluate the change of cathode and judge whether it is robust enough during the operation.”

R: We agree that this can give important information; unfortunately only one LSM/YSZ half cell sample was prepared for this study. We hope that this could be accepted in the revised version.

- “In the experimental section, author mentioned that the ASC technique detail using in this paper could not be given for patent right reason, thus the patent number should be mentioned herein.”

R: In section 2.1, when the ASC method is mentioned, the patent number is referenced right after, in the reference nº 24. Nevertheless, we inserted the patent number further in the same paragraph.

- “The LSM cathode prepared using ASC method possesses smaller particle and high porosity, it seems that the electrode may present high cathode performance in SOFC or half-cell test, however, the obtained ASR value is not as low as expect, why?”

R: By adding new references, we tried to make a more clear explanation on the high ASR founded in our sample. You may see this discussion on the paragraphs right before the conclusions.

- “The sentence, "It is related to the cathode/electrolyte charge and mass transfer from the LSM films to the YSZ", is not a proper expression. Charge transfer is a right concept to describe electrochemical reaction process, however, mass is a transportation process in fact.”

R: This sentence was modified in the revised version, according to your comment.

- “There is an obvious change between 550 C and 650 C as shown in Fig. 6. Author listed many related literature data herein, but mechanism explanation according to this work is absence in fact since the micro-structure of LSM cathode in this work is quite different from the references, while it may be changed during heating-up or cooling-down process to influence the electrode performance.”

R: The electrode processes mechanism proposed in our work is based on the reports of many authors, considering the similarities between the electrochemical behaviors of similar samples. Yet, changes in the microstructural features of the LSM catalyst can induce modifications in the activation energy values. In our paper the reaction mechanism adopted is shown in Fig. 5, together with a detailed explanation on the relation between experimental data and the fit and simulation process.

REVISOR #3

- “This manuscript concerns of using airbrush method for preparing thin film LSM cathode. Similar method for cathode preparation has been reported

in https://doi.org/10.4028/www.scientific.net/MSF.727-728.669. It is interesting as an alternative way for fabricating SOFC cathodes."

R: The paper is interesting, but it deals with an airbrushed LSM suspension deposited on an YSZ substrate and fired at high temperature (1200°C), and focus more on the rheological properties of the organic suspension, rather than the microstructure and electrochemical performance. The method used in our work uses the deposition of an aqueous monophasic solution and a low temperature thermal treatment (850°C). Nevertheless, we added the mentioned paper as a reference in the revised version, as a comparison for the film thickness.

- "In the characterization part, how the impedance been measured, how is the sample looks like, is it a symmetrical cell? what is the material for the counter electrode?"

R: In the revised version we enhanced the description of the experimental procedure carried out in the impedance analysis and added a schematic drawing of the sample testing. The YSZ/LSM sample is a half-cell, as mentioned many times along the paper and also in the title of section 2.1. The counter electrode is the contact electrode itself, which is a gold sputtered layer in the YSZ side of the half-cell.

- "In Figure 2a, it is clear that the YSZ subtract has quite a rough surface, would this influence the interface between LSM nano particle and the substrate, how would this influence the thin file preparation and the electrocardiogram performance?"

R: Yes. We analyzed this point more carefully in the revised version and, not only the surface roughness, but also the existence of lamination cracks in the YSZ bulk could have been responsible for the high ASR value measured.

- "If the LSM film was made at 850C, and is there any degradation/particle growth during testing at 850C?"

R: We believe that it was not the case. We based ourselves in our earlier work where the sintering properties of LSM nanopowders were studied and also another reference was added to the revised version.

- “In 3.3 How did the author get the LSM/YSZ half cell EIS spectra(Figure 4.a)? This should be detailed also in the characterization part.”

R: In the revised version we enhanced the description of the experimental procedure carried out in the impedance analysis.

- “Au was sputtered as contact electrodes, what is the thickness of the Au, would the Au influence the electrode performance?”

R: We have tested the influence of the gold cover thickness in the EIS results. With no or very thin Au cover (80 nm), an extra impedance arc was founded in the Nyquist plots. While thicknesses of ~350 nm eliminated this extra arc, and that is what was used in the paper.

- In Figure 4.a, the author use two RQ element for modeling of the EIS, how the author determine the Rsuf and Rint? usually numerical modelling does not necessarily correlated to the physical process, beside temperature variation, O2 partial pressure variation should be performed to better separate the Rint and Rsuf process.

R: We agree that O2 pressure variation could bring more on the electrochemical results, but we had no equipment to do so at the time. Instead, we were based on references that tested the O2 pressure variation in similar samples and temperatures. In Fig. 5 we explained our considerations on the relation between reaction mechanisms, fitting and simulation of EIS experimental results and the literature and state-of-the-art of LSM/YSZ half-cell electrochemical properties.

- “As the author listed the ASR values from the literature. The ASR of this work is more than 10 times of the literature reported value, which significantly weak the scientific discussion of the work such as Ea values and the comparison with the other literature. What is the reproducibility of the results? The author claims that the the low adherence, interface contact etc as possible reasons, is there any evidence to support this? seen from the cross section SEM in Figure 3a, it looks they have a quite good adherence between the two phases. And if it is due to contact loss, it has to be at least a factor of 10 times loss of contact. what is the ohmic resistance of the YSZ electrolyte used

here? The author should compare the ohmic resistance with the measured resistance of the cell.”

R: We enhanced the discussion in section 3.3 of the revised paper and these issues were addressed.

HIGHLIGHTS

1. The novel Airbrushed Solution Combustion (ASC) deposition method was tested.
2. A thin LSM film with average grain size of 55 nm and 10 μm thick was obtained.
3. A very thin and interconnected porosity was observed in the nanostructured film.
4. Electrochemical phenomena were separately related with microstructural features.
5. O_2 reduction steps had low activation energies but high area specific resistance.

DEPOSITION OF NANOSTRUCTURED LSM PEROVSKITE THIN FILM ON DENSE YSZ SUBSTRATE BY AIRBRUSHED SOLUTION COMBUSTION (ASC) FOR APPLICATION IN SOFC CATHODES

ABSTRACT

To make SOFC high efficiency energy generation devices, thin ceramic films are proposed as their main components. The rate of the oxygen reduction reaction is relevant for the overall performance of the SOFC, hence a lot of attention is given to the cathodes and their interfaces. The airbrushed solution combustion (ASC) method was used to fabricate an LSM thin film on a dense YSZ substrate. A single phase LSM perovskite was obtained with very thin and interconnected porosity, and a small average grain size (55 nm). The nanostructured LSM thin film electrode showed a low total activation energy (1.27 eV) at high temperatures, but a high area specific resistance at 850°C (55 Ω.cm²). The activation energy for the dissociative adsorption and diffusion of oxygen was significantly low (1.27eV), while the charge transfer and oxygen ion migration activation energy at the LSM/YSZ interface (1.28 eV) was closer to those usually reported.

KEYWORDS: LSM perovskite; nanostructured cathode; SOFC; oxygen reduction reaction; airbrushed solution combustion (ASC).

1. INTRODUCTION

High efficiency energy conversion devices are often referred to as vital for the construction of a sustainable grid based on distributed energy. In this sense, solid oxide fuel cells (SOFC) can play an important role in the near future, due to their great potential as an efficient energy generator, combined with low levels of emissions [1,2]. Nowadays, a few large enterprises already dispose of SOFC systems as their energy supplier, however, substantial use of this technology is yet to come. This is due to the

costs involved in the fabrication and in the maintenance of the SOFC energy banks, which usually requires very specialized labor. Also, their performance and reliability, which are very important commercial factors, are closely related to the fabrication process and component design [3]. In the most recent generation of SOFC devices, the intermediate temperature SOFC (IT-SOFC), the operating temperature is potentially reduced to the range of 500°C to 750°C. The main components are formed by thin films, deposited over each other, in order to form the SOFC stack. The mechanical support of the set is made by the interconnector which, due to the low operating temperature, can be composed of a metallic alloy [4].

Different methods can be used to fabricate thin films for IT-SOFC devices. Techniques based on vapor deposition and those involving the use of plasma, usually allow good microstructure and thickness control of the obtained films and can be conducted using a great variety of materials [5,6]. However, they generally require the use of robust and precise equipment and, in some cases, high processing temperature and expensive raw materials [7,8]. Thin films used in SOFC are also obtained by the processing of ceramic powders. Methods such as tape casting, screen printing, dip coating and spin coating, amongst others, are frequently reported as potential paths for the manufacturing of SOFC devices with low cost equipment and simple technological transfer [9]. The microstructure is controlled by the characteristics of the slurry, which is significantly influenced by the characteristics of the starting powder. Also the use of high sintering temperatures (> 1000°C) is common [10–12]. Precursor solution based methods perform a one-step synthesis and deposition of ceramic materials on the surface of different substrates [13,14]. In such methods, lower processing temperatures can be used and sufficient microstructural control is managed, by selecting suitable experimental conditions [15].

Considering that the cathodic reaction, which is the oxygen adsorption and its reduction and injection in the ion conducting electrolyte, is reported as the limiting factor of the overall SOFC performance, it is important that proper compositional and structural characteristics are achieved through processing [16,17]. Strontium-doped lanthanum manganites (LSM) are the most commonly used materials to compose the cathode in the SOFC. They present chemical and physical compatibility with yttria-stabilized zirconia (YSZ), which is a material generally used as an electrolyte, in typical

operating and processing temperatures of SOFC devices [18,19]. Composite electrodes based on LSM have also been tested for use in cells with YSZ electrolytes [20–22]. A better cathode performance can be achieved when its porous microstructure optimizes the air flow in its interior and, even more important, increases the active sites for the reaction by the enlargement of the triple phase boundary (TPB) zone [23]. Also, the contribution of the gas transport of molecular oxygen to the total cathode polarization is insignificant in thin films with relatively high porosity [24]. More recently, other cathode characteristics such as the length of the adsorption/diffusion process and surface diffusivity of oxygen adsorbed atoms have also been given importance, and they have a close relation with the physical properties and microstructural parameters of the cathode [25]. With the production of a nanostructured component, with small grain and pore size, a decrease in the activation energy may be attained, improving the cathode performance and, consequently, the overall performance of the SOFC device [17,21,26].

In this work, an attempt was made to obtain a LSM thin film with optimum porous microstructure and reduced grain size. The Airbrushed Solution Combustion (ASC) method [27] was tested to fabricate an LSM/YSZ half-cell, by depositing a thin LSM film on a dense YSZ substrate. Structural and morphological characterization of the LSM film was carried out and its electrochemical properties were evaluated in respect to the oxygen reduction reaction mechanism to verify the suitability of the deposition method.

2. EXPERIMENTAL

2.1 Preparation of the half-cell

In order to fabricate the substrate, YSZ powders (Sigma-Aldrich – 99.9%) were mixed in distilled water containing 2.5 wt.% of polyvinyl alcohol (Vetec-Brasil – 99.0%), to act as a binder. After drying for 24 h at 110°C the mixture was sieved using #60 mesh and separated into a portion of 650 mg. It was then submitted to 175 MPa in a uniaxial press using a 12 mm diameter mold. The sintering of the substrate was carried

out in air, using a heating rate of 10°C/min up to a 1450°C plateau, where it was held for 90 min.

A 15 mol% of strontium was chosen as the A-site dopant in the lanthanum manganite thin film, resulting in the $La_{0.85}Sr_{0.15}MnO_3$ compound . Higher Sr ratios are not advisable because it increases the thermal expansion which can make it incompatible with the YSZ substrate [28]. Besides, in amounts up to 15 mol%, Sr^{2+} cations are chemically more stable due to their lower diffusion rate into YSZ electrolytes [29].

The LSM film was deposited on the dense YSZ substrate by the Airbrushed Solution Combustion (ASC) method [27]. The ASC is based on precursor solution techniques with metal salts and organic fuels and with a relatively low processing temperature. In this work, the LSM film was deposited at 650°C and subsequently heat treated at 850°C for 3 hours with a heating and cooling rate of 2°C/min. Further investigations on the ASC deposition of porous ceramic films are being carried out and, also because of patent (BR 10 2017 008343 8 A2) rights, no further details of the deposition step can be given.

2.2 Characterization

The YSZ substrate had its apparent porosity, apparent density and densification determined by the Archimedes method [30]. The rate of densification was calculated considering the mass and volume of the samples and the theoretical density of YSZ as 6.10 g/cm³.

Room temperature X-ray diffraction (XRD) patterns of the YSZ substrates and of the LSM film were collected using a Bruker ASXD8 Advance equipment, in the range (2θ) of 20° to 70° with a 0.05° step and a 2 s capture time. The obtained patterns were compared with the International Centre for Diffraction Data (ICDD) database using the X'pert Highscore tool.

The microstructure of the YSZ substrate, as well as the deposited LSM film, was evaluated with a Hitachi TM-1000 table top scanning electron microscope (TT-SEM). Low magnification micrographs were used to evaluate the YSZ surface and the presence of cracks and continuity of the film. For a more detailed microstructural

observation of the LSM film a Hitachi S-4700 field emission SEM (FEI-SEM) was used. For this analysis the film was initially gold sputtered. After the electrochemical analysis, the half-cell was cold embedded with epoxy resin and cut in half with a diamond disc. The cross sectional observation of the half-cell was carried out in a Zeiss EVO MA10 scanning electron microscope (SEM) with a coupled Energy Dispersive Spectroscope (EDS) detector, and an EDS line scan measurement was performed along the LSM/YSZ interface.

Before the electrochemical impedance spectroscopy (EIS) characterization, the LSM/YSZ half-cell received a sputtered gold cover of a few hundreds of nanometers on both sides, acting as contact electrodes. A Metro-ohm Autolab equipment, internally coupled with a radio frequency analyzer, uses two platinum probes in contact with each side of the gold sputtered faces of the half-cell. Figure 1 shows a scheme of the sample analyzed by EIS. The measurements were done in a furnace, under air atmosphere and at temperatures from 450°C to 850°C, with steps of 50°C and a heating rate of 5°C/min. The frequency range used was from 10^{-2} Hz to 10^{6} Hz, increasing in a logarithmic scale and with AC signal of 50 mV. The collected data was analyzed using the Nova 1.10 software, where the Nyquist plots were fitted and simulated using equivalent circuits, based on electrochemical reaction mechanisms.

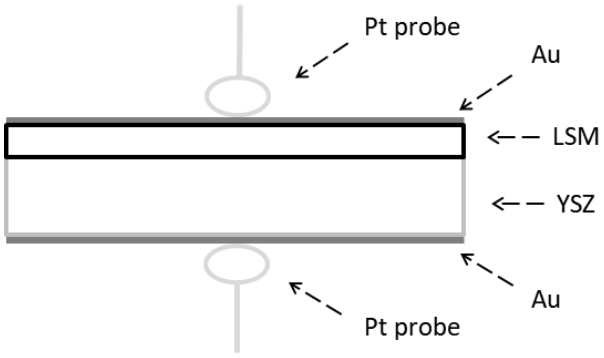

Figure 1: Scheme of the LSM/YSZ half-cell during the EIS analysis.

3. RESULTS AND DISCUSSION

3.1 Phase formation

The sintered YSZ substrate was 1.2 mm thick and 10 mm in diameter. The apparent porosity was determined as 1.44% and the apparent density was 5.99 g/cm³, which compared to the considered theoretical density (6.10 g/cm³), is only 1.8% lower. For this type of substrate a densification of more than 95% is desirable, considering its function as an ion conductor electrolyte and a physical barrier for the separations of gases in the SOFC [28]. The substrate reached a densification of 96.3% and, therefore, attained the required standard for a satisfactory deposition and characterization of the LSM thin film. The densification is slightly lower than the apparent density (98.2%), which may be due to closed pores in the substrate.

In Figure 2.a, an XRD pattern of the obtained YSZ substrate is shown with identified peaks marked. This pattern matched with the ICDD 01-089-9069 file, which corresponds to the cubic structure of zirconium oxide. This phase is the one that shows the higher ionic conductivity and is stabilized at low temperatures by the addition of yttrium oxide [31].

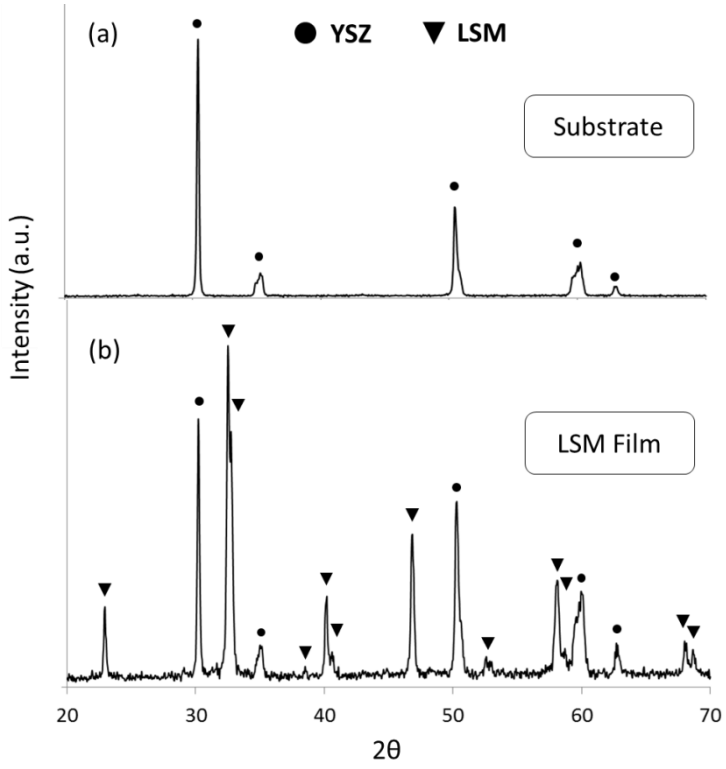

Figure 2: XRD pattern of (a) YSZ substrate and (b) LSM film.

The XRD pattern of the LSM film is shown in Figure 2.b. YSZ peaks are found amongst LSM peaks and are identified with different marks. The LSM film matched file is ICDD 01-089-0648, which corresponds to the rhombohedral perovskite structure. It is known that the addition of bivalent cations, such as Sr^{2+}, in lanthanum manganites induces the formation of Mn^{4+} species. Gaudon et al. [32] studied the influence of dopant concentration on the structure of LSM compositions. It was observed that the concentration of Mn^{4+} ions in the LSM structure is constant for Sr^{2+} amounts of up to 30%. In this composition range, the Mn^{4+} remains at a concentration of around 40% and maintains stable the LSM rhombohedral perovskite structure.

Another important factor is the LSM thermal history. Considering the same strontium amounts (up to 30%), Cortes-Gil et al. verified that when thermally treated below 1000°C, the LSM rhombohedral structure is stable, whereas at higher temperatures the orthorhombic structure is stabilized [33]. In a previous study a heat treatment at 750°C also kept the LSM rhombohedral structure stabilized. Hence, when processing the LSM with such a composition at relatively low temperatures, this structure is more likely to be found [34].

3.2 Morphology

A TT-SEM micrograph of the YZS substrate surface is shown in Figure 3.a. The observed microstructure is composed of sub micrometric grains and the presence of some porosity can also be seen. Despite of these pores, the YSZ substrate microstructure was considered suitable to continue to the film deposition stage, based also on the aforementioned XRD and densification results. The FE-SEM micrograph in Figure 3.b presents a good surface sample of the LSM film deposited on the YSZ substrate. A continuous and porous film is observed. Insignificant remnants of cracks may be seen in the film, which is practically crack free. Gharbage et al. [6] compared an LSM film deposited by ultrasonic spray with an RF sputtered one, both with a final thermal treatment at 900°C, and observed that the first method led to the formation of cracks with sizes between 1 to 10 µm, while with the second method the film structure seemed denser, with few pores.

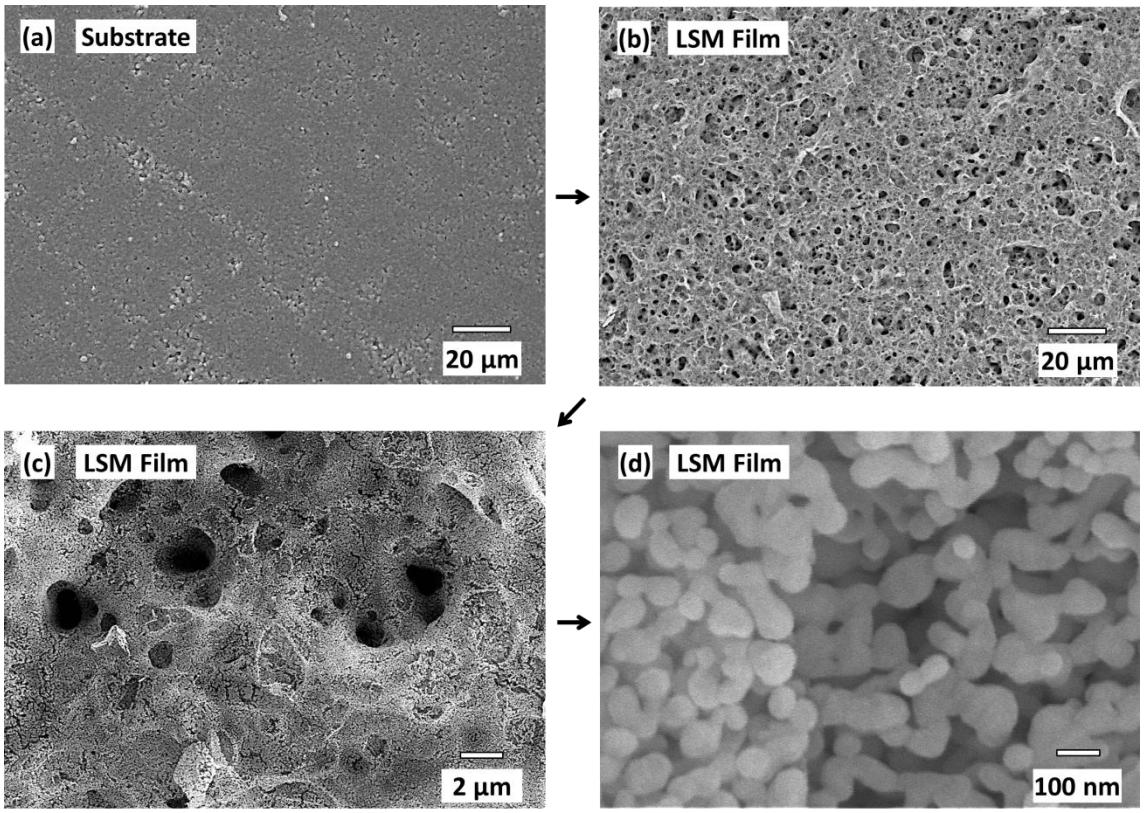

Figure 3: TT-SEM micrograph of the (a) YSZ substrate and FE-SEM micrographs of the (b, c and d) LSM film at different magnifications.

Analyzing the FE-SEM micrographs, shown in Figures 3.c and 3.d, more details are revealed in the microstructure of the LSM film. Regarding the magnification increase in these FE-SEM micrographs, it is assumed that the LSM film obtained by ASC has different structural levels. In Figure 3.c, relatively large pores, with diameters of around 3 µm, are seen and, in a closer look (Figure 3.d), a much finer porosity is revealed. These small pores are very abundant throughout the microstructure and it can be seen that they are intensely interconnected, forming a porosity network. It is assumed that the porous nanostructure obtained by the ASC thin film deposition method can play a very important role in its application as an SOFC cathode, because it can potentially improve the gaseous permeability and impacts on the TPB extension and in the activation energy of the electrochemical reactions [23]. Brant et al. [35] observed that LSM grain growth and coarsening increases the pore size, leading to higher activation energy. Also, Niu et al. [36] observed that pore size distribution influences the current density and lifetime when surface cathode poisoning with foreign ions occurs. Su et al. [37] also mentioned the YSZ surface roughness as an

important factor for the electrochemical performance of LSM, because the formation of wider contact area enhances the TPB zone.

The average grain size of the LSM film obtained by ASC deposition and heat treated at 850°C for 3 hours, is 55 nm. Together with the deposition method and parameters, the temperature applied in the thermal treatment is crucial for the fabrication of nanostructured ceramic films. A minimum temperature is required for better phase crystallization, but an increase in the temperature used can also promote grain growth and, in some cases, may lead to crack formation in the thin film [38]. Table 1 shows the comparison between the processing temperature and method with microstructural features of different LSM films with close compositions. The use of an airbrush was tested by Chiba et al. [39] for the deposition of a LSM suspension on an YSZ electrolyte and the films was heat treated at 1200°C and reached a final thickness of 30 µm. Hayashi et al. [7] deposited LSM cathode compositions using radio-frequency sputtering and verified grain growth in the film from 20 nm to 150 nm, because of the need of a 1000°C heat treatment. It was also reported that after the heat treatment, the grain morphology was square-shaped. The use of powder processing methods tends to promote even more significant grain growth, because they require higher processing temperatures. The screen printing deposition of LSM powders obtained by co-precipitation, as performed by Jiang [40], resulted in a 360 nm average grain size when a 1150°C heat treatment was used. The same method was used by Das et al. [41], but the final thermal treatment was at 1000°C, and it was observed that the size of the grains was mostly submicrometric with some larger grains of 1 to 2 µm. Benamira et al. [42] tested a simple brush painting of a commercial submicrometric LSM slurry, followed by sintering at 1200°C, where the average grain size seems to be smaller than 500 nm. A similar procedure was followed by Seyed-Vakili et al. [26] that used an even lower sintering temperature (1100°C) but ended up with larger grains. On the other hand, this same temperature used by Brant et al. [35] to treat commercial LSM powder deposited through a painting process, resulted in an average grain size of 200 nm. The aerosol flame deposition performed by Im et al. [43] also needed a thermal treatment of 1200°C and produced an even larger grain growth, close to 800 nm. Darbandi et al. [21] performed a spin coating deposition of LSM powder with particles measuring from 20 to 50 nm and, after a low temperature

thermal treatment (850°C), the final grain size did not seem to have varied much, with an average size being close to 100 nm.

Table 1: Cathodic material, deposition method, processing temperature and microstructural features of LSM films found in the literature among with the one obtained by ASC.

Ref. n°	Cathodic material	Deposition method	Process temperature	Grain size (nm)	Thickness (μm)
*	$La_{0.85}Sr_{0.15}MnO_3$	ASC	850°C	55	10
[6]	$La_{0.5}Sr_{0.5}MnO_3$	RF sputtering	900°C	NA	1
[6]	$La_{0.5}Sr_{0.5}MnO_3$	ultrasonic spray	900°C	NA	10
[7]	$La_{0.5}Sr_{0.5}MnO_3$	RF sputtering	1000°C	150	0.6 – 1.2
[21]	$La_{0.75}Sr_{0.2}MnO_{3-\delta}$ [n]	spin coating	850°C	< 100 #	0.5
[21]	$(La_{0.8}Sr_{0.2})_{0.95}MnO3_{-\delta}$ [μ]	screen printing	1150°C	NA	10
[26]	$La_{0.8}Sr_{0.2}MnO_3$	painting	1100°C	~ 1000 #	40
[22]	$La_{0.8}Sr_{0.2}MnO_3$/20%YSZ	screen printing	1200°C	NA	35
[35]	$La_{0.65}Sr_{0.35}MnO_3$	painting	1100°C	200	NA
[39]	$La_{0.85}Sr_{0.15}MnO_3$	airbrushing	1200°C	NA	30
[40]	$La_{0.72}Sr_{0.18}MnO_3$	screen printing	1150°C	360	50
[41]	$La_{0.65}Sr_{0.3}MnO_3$	screen printing	1000°C	~ 1000 #	50
[42]	$La_{0.8}Sr_{0.2}MnO_3$	painting	1200°C	< 500 #	12
[43]	$La_{0.8}Sr_{0.2}MnO_3$	aerosol flame	1200°C	< 800 #	8
[44]	$La_{0.8}Sr_{0.2}MnO_3$	spin coating	1100°C	NA	10

** this work NA not available # estimated from micrographs*

The cross sectional SEM micrograph taken at the end of the experimental procedure, is displayed in Figure 4.a. The thickness of the LSM film is 10 μm and, amongst the fine porosity discussed above, flattened larger pores were observed. Also, the porous LSM film looks well adhered to the YSZ substrate. In general, the techniques used for LSM deposition are versatile with respect to film thickness, as depicted in Table 1. Usually, sputtering methods allow the production of thinner films, of around a few micrometers or even less [6,7]. Through powder processing methods of LSM, or LSM/YSZ composites, it is more common to find thicknesses of a few dozen

micrometers [22,26,40,41]. Nevertheless, films with reduced thickness can also be achieved by conventional powder processing, as demonstrated by the brush painting and the spin coating performed by Benamira et al. [42] and Murray et al. [44], where the produced films were 12 and 10 µm thick, respectively. In some cases, ultrathin LSM films can be obtained by conventional powder processes, like the spin coating performed by Darbandi et al. [21], which resulted in a 0.5 µm thick film. Methods based on wet chemistry are also used in the production of thin LSM films. Gharbage et al. [6] used ultrasonic spray deposition and obtained a 10 µm thick LSM film, and Im et al. [43] reached 8 µm in a LSM film deposited by aerosol flame deposition. An study accomplished by Andersson et al. [45], using numeric modelling, demonstrated that 90% of the electrochemical reactions occur within a distance of 10 µm from the electrode/electrolyte interface and that thicker components may only increase ohmic losses. Also, Carpanese et al. [24] demonstrated that the polarization due to O_2 diffusivity is some orders of magnitude lower that the total cathode polarization in films as thin as 3 µm. The material costs also depend on the film thickness and can be reduced along with it. Hence, it is advisable that cathode thickness is less, or not much more, than 10 µm. In this sense, compared with data shown in Table 1, the LSM film thickness obtained by ASC deposition was considered suitable.

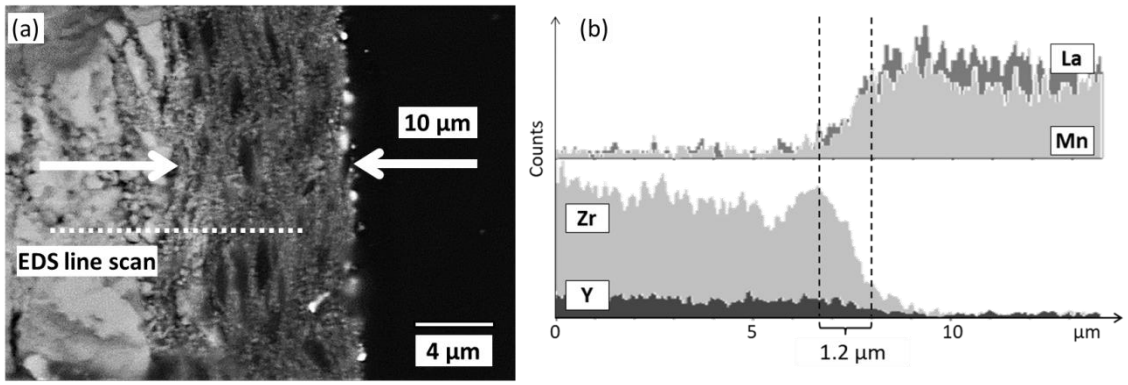

Figure 4: (a) Cross sectional SEM micrograph of the LSM thin film and (b) EDS line scan profile for the major elements.

In Figure 4.b the EDS line scan result is shown. The variation of the relative amounts of the main components of the substrate and the film were measured. Analyzing the elemental profile obtained from the YSZ substrate side, a high concentration of Zr in contrast with Y is observed, as expected. In the LSM film side,

the concentrations of La and Mn are similar. Considering the highest peaks of Zr, La and Mn near the interface it, was possible to determine a gradual transition of elements with a width of 1.2 μm. This may represent a region with more intense electrochemical activity or, less likely, due to the low heat treatment temperature (850°C), a dielectric phase formation process. Ananyev et al. [46] studied the cation interdiffusion in LSM/YSZ composite cathodes and observed a much smaller width of variable composition. It was determined that at high temperature exposure, this transient area tends to grow with time.

3.3 Electrochemical characterization

The measurements performed by the EIS technique can be used to determine the activity of catalysts in terms of an interfacial polarization resistance of a solid electrode/electrolyte interface. Such a relation occurs due to the similarity of the electrochemical behavior with an electrical circuit formed, essentially, by resistive and capacitive elements and, in some cases, inductive elements also. This implies that each electrochemical phenomenon presents a conservative element, independent of the frequency, in addition to the dissipative one. In this sense, the relative capacitance of a constant phase element can indicate the nature of an electrochemical phenomenon associated with a determined resistance [47,48]. Usually, the response of an LSM porous film deposited on an YSZ substrate is considered as two semi-circles in the Nyquist plot. The influence of temperature and microstructure at atmospheric pressure (pO_2 = 0.21 atm) on the overall cathode behavior was analyzed considering the separate influence of each phenomenon represented by a semi-circle in the impedance spectrum.

Figure 5.a shows the EIS spectra of the LSM/YSZ half-cell obtained at 550°C and 600°C. For the resistance values of both axes in the Nyquist plot, the area of the contact electrode was considered such that all the results are shown in terms of area specific resistance (ASR) and are designated solely with the letter R. In all measured temperatures up to 550°C, a small arc is observed in the high frequency region, followed by a larger arc composed by two overlapping semi-circles. At temperatures of 600°C and above, only the larger arc is observed. For this reason, the equivalent circuit

used to fit the experimental data for the spectra obtained at temperatures up to 550°C, is different from those obtained at temperatures of 600°C and above. At lower temperatures (T < 550°C), the equivalent circuit is composed of a serial resistance Rs connected to three RQ systems, where each RQ is a resistance R in parallel with a constant phase element Q. However, at higher temperatures (T > 600°C) there are only two RQ systems connected to Rs, as illustrated in Figure 5.b.

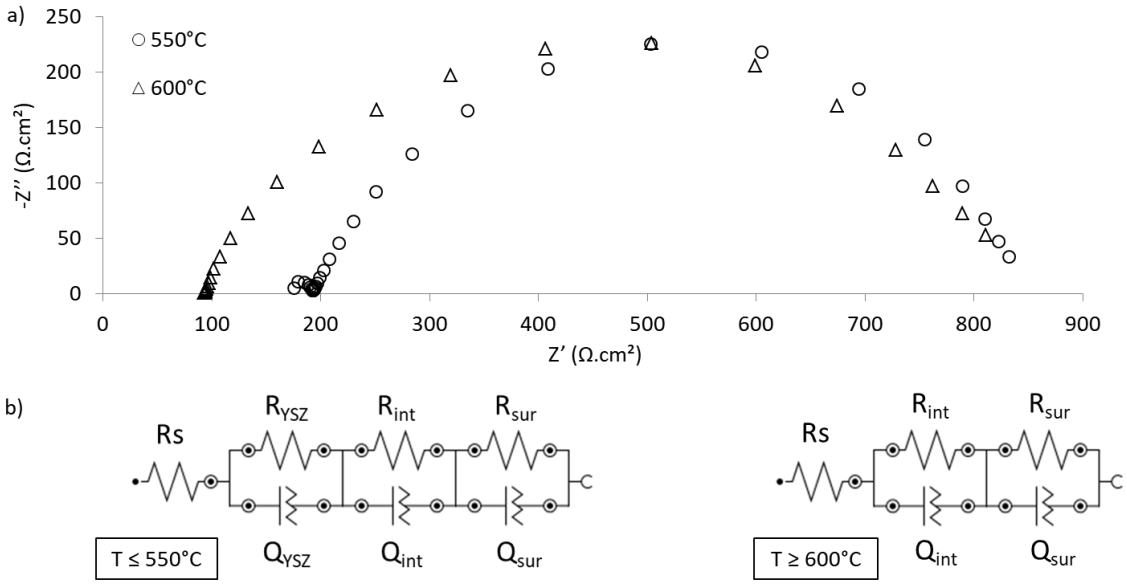

Figure 5: (a) Impedance experimental data at 550°C and 600°C and (b) equivalent circuits for different temperatures.

As 550°C is considered a relatively low temperature, besides the serial resistance (Rs), the high frequency RQ system can also be attributed to an electrolytic process and is represented as $(RQ)_{YSZ}$. The Q_{YSZ} element of the half-cell studied presented a capacitance value in the order of 10^{-9} F/cm². This value is within a range of capacitance associated with grain boundary processes suggesting that R_{YSZ} corresponds to the oxygen ion conduction resistance in the grain boundary of the YSZ electrolyte. Therefore, the Rs resistance in such temperatures represents the resistance inside the YSZ electrolyte grains [31,48]. This same behavior where the high frequency arc tends to lose its capacitive element with increasing temperature, has been reported in the literature [40,43]. The temperature where the $(RQ)_{YSZ}$ disappears depends, mainly, on the properties of the electrolyte and it can vary from under 600°C to temperatures just

above 700°C. In this process, the R_{YSZ} becomes part of the Rs and, at high temperatures, the Rs corresponds to the total ohmic resistance of the YSZ electrolyte.

The larger arc is associated with electrode processes and can be decomposed into two overlapped semi-circles, as reported by different authors [21,22,35,40,42,43]. Running the simulation of the obtained data considering two RQ systems in the half-cell, a capacitance in the order of 10^{-4} F/cm² is found in the lower frequency arc. This value indicates electrochemical reactions. In this case, it is attributed to the reactions and diffusion on the LSM surface, corresponding to the $(RQ)_{sur}$ elements. The other arc considered at intermediate frequencies has a capacitance in the order of 10^{-5} F/cm², which is a typical value for an interface process. It is related to the cathode/electrolyte charge transfer from the LSM films to the YSZ [40,43,48]. The interface elements are called $(RQ)_{int}$.

The reaction mechanism adopted by different authors assumes that four steps can take place in the LSM/YSZ half-cell. At first, the gaseous O_2 penetrates the porous LSM structure and is adsorbed in a favorable site on the LSM surface (O_{ads}). The adsorption promotes the O_2 molecule dissociation, using electrons from the external circuit. The dissociated O^- diffuses on the TPB area and proximities, towards the YSZ electrolyte. Once it finds an oxygen vacancy in the YSZ lattice, it undergoes the complete reduction to O^{2-} and it is fully incorporated in the electrolyte. For a better understanding of the relationship between the reaction mechanisms, the data generated by the impedance spectrum, and the fit and simulation treatment with equivalent circuits, a schematic illustration is shown in Figure 6. The dots are the experimental results obtained at 550°C, and the full line connecting them is the simulation result obtained with the software. Drawn below this curve are the semi-circles considered for the fit and simulation. In this model, the RQ elements of the electrode, $(RQ)_{int}$ and $(RQ)_{sur}$, can represent more than one reaction step, if compared to the mechanism described earlier. The resistance R_{sur} is associated with the dissociative adsorption of oxygen and diffusion, while the R_{int} resistance is related to the complete reduction of oxygen and injection in the YSZ electrolyte lattice.

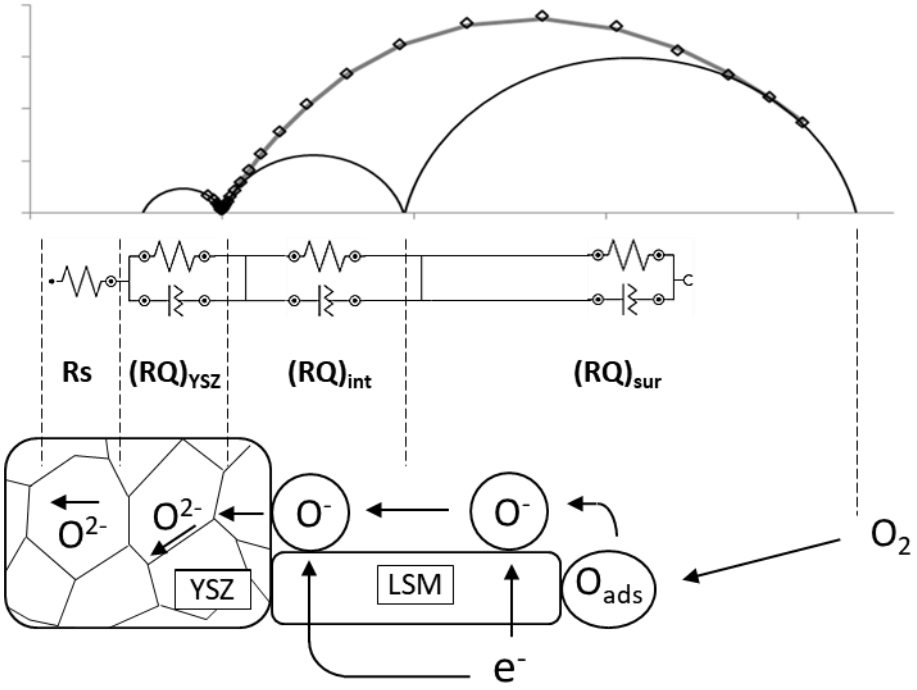

Figure 6: Scheme of the relationship between the impedance spectrum, the equivalent circuits, and the electrochemical reaction mechanism of oxygen reduction in the LSM/YSZ interface and nearby.

Figure 7 shows the Arrhenius plot of the overall electrode area specific resistance (R_e), which is the sum of R_{sur} and R_{int}, and represents to total charge transfer polarization of the electrode process [21,41]. A change in the curve slope is observed and starts at 550°C, where R_e remains virtually constant until 650°C. From this temperature on, the decrease in R_e occurs with different behavior, which means that there is a variation in the total activation energy of the electrode (Ea_e). At lower temperatures (T < 550°C) the Ea_e is 1.05 eV, and above 650°C, it is increased to 1.27 eV. As the oxygen reduction in the LSM/YSZ pair occurs through various reaction steps, this change can be attributed to a shift in the rate determining step of the overall reaction. Jiang et al. [22] stated that a theoretical variation in anodic and cathodic charge transfer coefficient can occur at a temperature around 700°C. The author attributed this deviation to the rate determining step shift and demonstrated experimentally the temperature influence on the Ea_e of LSM/YSZ composite cathodes, obtaining 1.33 eV at lower temperatures (T < 700°C), and 1.59 eV at elevated temperatures, above 700°C. Benamira et al. [42] observed a similar variation in the Ea_e of pure LSM cathode, where a deviation of Ea_e from 1.00 eV, up to 480°C, to 1.92 eV at

higher temperatures (T > 510°C), was observed. It is noted that the shift of the rate determining step can take place at a range of temperatures, with different shift temperatures being found in the literature. The starting temperature (550°C) and the Ea_e at low temperatures (1.05 eV) are close to those reported by Benamira et al. [42]. While at higher temperatures (T > 650°C) the obtained value of Ea_e (1.27 eV) and the electrode behavior change temperature are nearest to those reported by Jiang et al. [22]. Barbucci et al. [49] observed that the addition of YSZ to the LSM cathode only influenced the polarization resistance, and did not influence the activation energy, where an Ea_e of around 1.04 eV (T > 700°C) was verified for pure LSM and for cathodes with different amounts of YSZ. This statement corroborates an earlier study carried out by Murray et al. [44], where it is also inferred that the presence of YSZ in the LSM electrode does not change the rate determining step and, consequently, does not change the Ea_e. Nevertheless, they reported a slight decrease in the Ea_e from 1.61 eV for pure LSM, to 1.49 eV for LSM/50%YSZ composite. The possibility of the shift in the Ea_e have been caused by grain growth or microstructural modifications was discharged, since it is reported to occur only at temperatures above 1000°C, even for powders with reduced grain size [50,51].

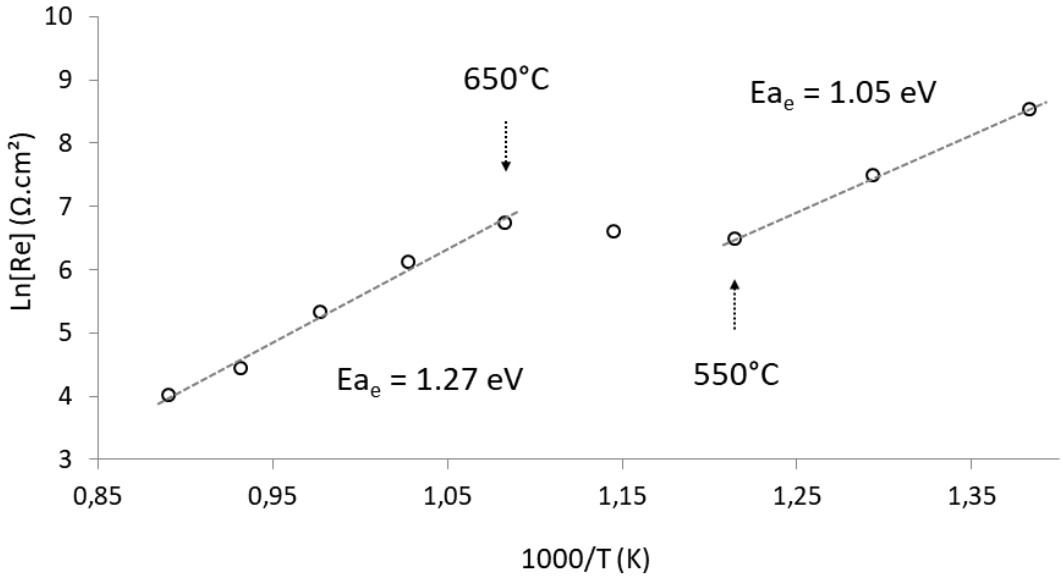

Figure 7: Variation of the overall electrode resistance (R_e) of the LSM thin film with temperature.

Table 2 brings together the electrochemical characteristics of the LSM electrode deposited by the ASC process with other results reported by different authors with various cathode compositions. Values of Ea_e at high temperatures, near 2.00 eV, can be found in the literature as well as values closer to 1.00 eV. This is because many variables can influence the total Ea_e, like the morphological aspects, the actual composition of the LSM thin films, adherence and contact with the YSZ substrate, and also its electrolytic characteristics. Although some authors correlate the LSM thin film microstructure with the activation energy and total polarization, in the studies referred to this work, a direct and general correlation of these factors is not easily observed due to divergence or lack of information. Lee [52] screen printed an $La_{0.5}Sr_{0.5}MnO_3$ thin film on an YSZ substrate and obtained an Ea_e of 1.76 eV (T > 600°C) with a firing temperature of 1100°C. Yang et al. [53] used the same method, with a firing temperature of 1150°C, to deposit a $(La_{0.8}Sr_{0.2})_{o.97}MnO_3$ thin film and found a similar Ea_e value of 1.80 eV (T > 800°C). When the substrate was changed to samarium-doped ceria, the Ea_e decreased to 1.47 eV, highlighting the influence of the electrolyte on the overall electrode activation energy (Ea_e). The influence of annealing temperature of $La_{0.65}Sr_{0.35}MnO_3$ thin films was reported by Brant et al. [35]. When fired in temperatures up to 1200°C, the Ea_e obtained was near 1.20 eV, and above these temperatures a gradual increase was observed, attributed to the loss of porosity of the thin film and also to the formation of secondary phases in the LSM/YSZ interface, with the Ea_e reaching up to 2.00 eV. Compared with these works, the high temperature Ea_e of the LSM thin film deposited by ASC (1.27 eV, T > 650°C) can be considered low and it is likely that this fact is related to the influence of the morphological characteristics of the thin film, such as small grain size and fine interconnected porosity. Darbandi et al. [21] compared LSM cathodes obtained from commercial micro LSM powder with a synthesized nanopowder and reported a reduction in the Ea_e from 1.52 to 1.41 eV (T > 500°C). For a similar commercial LSM starting powder, Seyed-Vakili et al. [26] obtained the same value of Ea_e (1.52 eV), whereas the film was sintered at 1150°C, which is 50°C higher.

Table 2: Electrochemical properties of LSM thin film deposited by ASC, amongst those reported by different authors.

Ref. n°	Cathodic material	Temp. range	Ea_e (eV)	Ea_{int} (eV)	Ea_{sur} (eV)	ASR-850°C (Ω.cm²)
*	$La_{0.85}Sr_{0.15}MnO_3$	< 550°C	1.05	0.86	1.37	NA
*	$La_{0.85}Sr_{0.15}MnO_3$	> 650°C	1.27	1.28	1.27	55
[21]	$La_{0.75}Sr_{0.2}MnO_{3-\delta}$ n	> 500°C	1.41	NA	NA	0.62
[21]	$(La_{0.8}Sr_{0.2})_{0.95}MnO_3$ μ	> 500°C	1.52	NA	NA	2.32
[21]	$La_{0.75}Sr_{0.2}MnO_{3-\delta}$/25%GDC	> 500°C	1.13	NA	NA	0.06
[26]	$La_{0.8}Sr_{0.2}MnO_3$	> 600°C	1.52	NA	NA	6.71 [-]
[35]	$La_{0.65}Sr_{0.35}MnO_3$	> 900°C	1.20-2.00	NA	NA	NA
[37]	$(La_{0.75}Sr_{0.25})_{0.95}MnO_{3-\delta}$	800°C	NA	NA	NA	7.59 [-]
[40]	$La_{0.72}Sr_{0.18}MnO_3$	> 700°C	2.22	1.13	3.04	6.2 [+]
[42]	$La_{0.8}Sr_{0.2}MnO_3$	< 500°C	1.00	NA	NA	NA
[42]	$La_{0.8}Sr_{0.2}MnO_3$	> 500°C	1.92	NA	NA	NA
[43]	$La_{0.8}Sr_{0.2}MnO_3$	> 600°C	1.48	1.60	1.38	1.7 [+]
[22]	$La_{0.8}Sr_{0.2}MnO_3$ / 20% YSZ	< 700°C	1.33	NA	NA	NA
[22]	$La_{0.8}Sr_{0.2}MnO_3$ / 20% YSZ	> 700°C	1.59	NA	NA	12 [#]
[44]	$La_{0.8}Sr_{0.2}MnO_3$	> 550°C	1.61	NA	NA	0.70 [#]
[44]	$La_{0.8}Sr_{0.2}MnO_3$ / 50% YSZ	> 550°C	1.49	NA	NA	0.09 [#]
[49]	$(La_{0.75}Sr_{0.25})_{0.95}MnO_{3\ddagger\delta}$	> 700°C	1.04	NA	NA	4.5 [#]
[52]	$La_{0.5}Sr_{0.5}MnO_3$	> 600°C	1.76	NA	NA	7.9 [#]
[53]	$(La_{0.8}Sr_{0.2})_{0.97}MnO_3$	> 800°C	1.80	NA	NA	3.8 [#]

** this work NA not available [#] estimated from Arrhenius plot [-]800°C [+]900°C*

A comparison between R_{int} and R_{sur} behavior with increasing temperature is shown in the Arrhenius plot of Figure 8. A change in the predominant behavior, together with a shift in the E_a of both reactions, is noted. At low temperatures (T < 550°C) the LSM/YSZ interface reaction is predominant, showing a higher ASR (R_{int}), while at higher temperatures (T > 650°C) the ASR of the LSM surface reaction (R_{sur}) has higher values. Im et al. [43] observed a similar transition of the predominant reaction occurring at slightly higher temperatures, in the range of 650°C to 750°C, assuming that R_{int} is related to the charge transfer resistance in the LSM/YSZ interface and R_{sur} to

the dissociative adsorption and diffusion of oxygen in the LSM surface. On the other hand, Jiang [40] reported a different behavior, where R_{sur} is predominant at lower temperatures while R_{int} has higher ASR values at higher temperatures, with the transition occurring around 800°C.

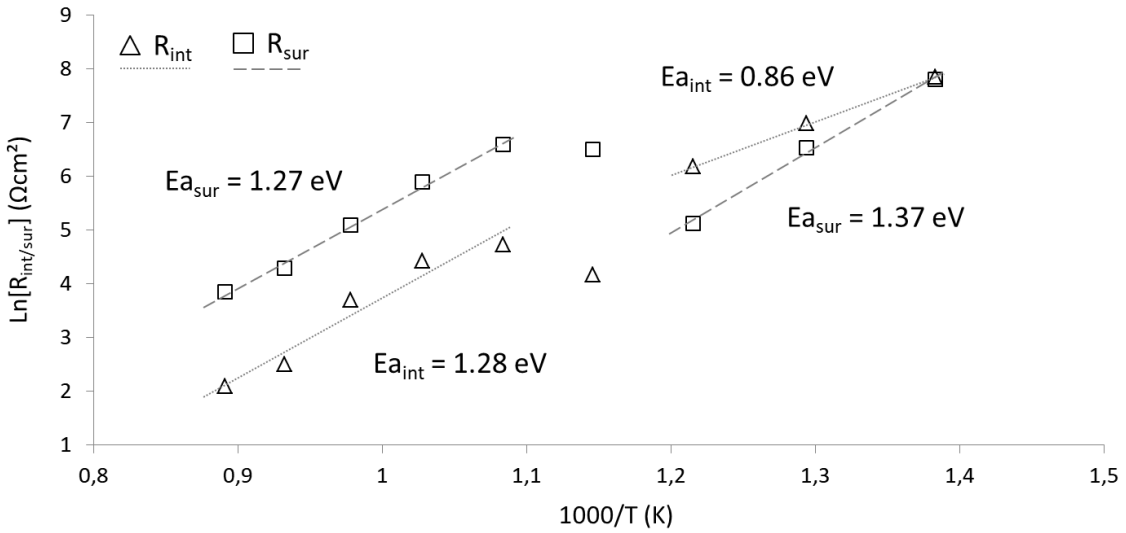

Figure 8: Arrhenius plot of Ri_{nt} and R_{sur}.

The activation energy of the LSM/YSZ interface (Ea_{int}) at temperatures lower than 600°C is 0.86 eV, and at higher temperatures increased to 1.28 eV. At the interface, charge transfer and oxygen ion migration take place. It is possible that a variation in the predominant step at R_{int} occurs from low to high temperatures [22,40,42]. Considering the E_{aint} at higher temperatures (1.28 eV), the obtained value is between the 1.13 eV, reported by Jiang [40], and the 1.60 eV obtained by Im et al. [43]. The activation energy of the LSM surface (Ea_{sur}) decreased from 1.37 eV to 1.28 eV with rising temperature. In this region, the dissociative adsorption and diffusion of oxygen are the considered steps [22,40,42] and, again, the temperature seems to influence the predominant one. At higher temperatures, the Ea_{sur} (1.27 eV) is lower than those in literature [40,43].

Considering the values of Ea_{int} and Ea_{sur} obtained at high temperatures and the microstructure observed in this study, compared with other works, it may be inferred that a thicker film, such as the one obtained by Jiang [40] with 50 µm, results in a higher value of Ea_{sur} (3.04 eV), while thinner films may cause a decrease in Ea_{sur}, as

seen in the report of Im et al. [43] (1.38 eV) with a thickness of 8 µm, and in this work where with a 10 µm thick film, an Ea_{sur} of 1.27 eV was achieved. The small grain size and fine interconnected porosity of the LSM film deposited by ASC may have influenced the relatively low Ea_{sur} obtained. These morphological aspects can also be related to low Ea_{int}. The Ea_{int} and average grain size of Jiang [40], and Im et al. [43], were 1.13 eV for 360 nm and 1.60 eV for 1 µm, respectively. In this work, an Ea_{int} of 1.28 eV was obtained for an average grain size of 55 nm and it is possible that these values could be lowered by improving the substrate quality and interface adhesion, as discussed below.

The total electrode ASR (R_e) is strongly influenced by measurement temperature and can undergo other variations due to structural characteristics, such as grain size, porosity, thickness and substrate material [21,26,35]. The R_e at 850°C obtained in this study (55 Ω.cm²) is relatively high when compared to results reported by other authors. Usually, R_e values remain under 10 Ω.cm², as shown in Table 2. Lee [52] and Yang et al. [53] screen printed LSM compositions with sintering temperatures of 1100°C and 1150°C and reported 7.9 Ω.cm² and 3.8 Ω.cm² at 850°C, respectively, which are already relatively high values. At the temperature of 900°C, Jiang [40] and Im et al. [43] reported R_e as 6.2 Ω.cm² and 1.7 Ω.cm², respectively. Lower ASR values can be achieved with the use of composite cathodes, such as in the works of Murray et al. [44], which tested LSM with 50% of YSZ and obtained 0.09 Ω.cm², and Darbandi et al. [21], which used LSM with 25% gadolinium-doped ceria and reached 0.06 Ω.cm². Barbucci et al. [49] observed that the addition of up to 50% YSZ to LSM cathodes decreased the ASR values, whereas, at higher concentrations the ASR showed an increase. The study with YSZ buffer layers, by Benamira et al. [42], indicates that the contact quality between components could directly influence the total electrode ASR. The use of a YSZ porous interlayer could also lead to better and broader LSM/YSZ interface contact, according to the study of Su et al. [37], where the use of such a layer decreased the total polarization resistance from 7.59 Ω.cm² to 2.19 Ω.cm², at 800°C. At this same temperature, Sayed-Vakili et al. [26] obtained 6.71 Ω.cm² by testing a commercial LSM material. Somehow, even with improved morphological characteristics and low values of Ea_e, the LSM film obtained by ASC presented high polarization resistance.

Considering the LSM nanostructure it was expected a decrease in both Ea_e and R_e. It is known that nanocrystalline materials can present a change in the energetic state of interfaces, including gas/solid and solid/solid interfaces [54,55]. This change in the interface energy can explain the promising Ea_e values reported in this work, since the activation energies depend directly on the surface energetic state. On the other hand, nanostructures also provide an increase in the active sites and defects concentration, as well as enhancement in thin films adherence and, consequently, a decrease in Re should have been observed [41,55], but in despite of it a high R_e value was found. It is possible that microstructural defects within the YSZ bulk have caused deleterious effects on the cathode performance, since it was already reported that nature and quality of the electrolyte can directly influence the cathode polarization;

The YSZ electrolyte is a pure ionic conductor and, in this work, the total conductivity of the electrolyte was found higher (0.048 S/cm) than the usually reported [56,57]. Kwon and Choi [57] reported that the difference between the conductivity of YSZ bulk and thin film is observed only when an across-plane current is tested, while in an in-plane current the conductivities are alike. In this sense, the lamination like defects observed in the electrolyte in Figure 4.a may be the cause of poor electrolyte conductivity and, consequently, high R_e of the LSM film.

4. CONCLUSIONS

A porous 10 µm thick nanostructured LSM film was deposited on a dense YSZ substrate by the ASC method. The film presented no secondary phases, being composed of crystalline LSM rhombohedral perovskite after heat treatment. Enhanced morphological characteristics were observed, such as very fine and interconnected porosity and an average grain size of 55 nm. The activation energy of the electrode, as well as the LSM/YSZ interface and LSM surface activation energies underwent an increase at temperatures higher than 650°C, but still remained low compared to the literature values, probably due to the morphological characteristics. The total electrode ASR (55 $\Omega.cm^2$) was considered high for the LSM/YSZ system, probably due to microstructural defects in the YSZ electrolyte that decreased its conductivity and,

hence, the cathode global performance. The development of nanostructured thin ceramic films using the ASC method is promising and further investigation must be carried out for optimum use of this novel deposition technique.

5. ACKNOWLEDGEMENTS

The authors would like to thank *Conselho Nacional de Desenvolvimento Científico e Tecnológico* (CNpQ) and *Coordenação de Aperfeiçoamento de Pessoal de Nível Superior* (CAPES) in Brazil and *Instituto de Cerámica y Vidrio* (ICV) and *Consejo Superior de Investigaciones Científicas* (CSIC) in Spain. Also, especial thanks to Dr. José Ramón Jurado who helped with the lead of our group in this research.

6. REFERENCES

[1] Stambouli AB, Traversa E. Solid oxide fuel cells (SOFCs): a review of an environmentally clean and efficient source of energy. Renew Sustain Energy Rev 2002;6:433–55. https://doi.org/10.1016/S1364-0321(02)00014-X.

[2] Omer AM. Green energies and the environment. Renew Sustain Energy Rev 2008;12:1789–821. https://doi.org/10.1016/j.rser.2006.05.009.

[3] Weimar MR, Chick LA, Gotthold DW, Whyatt GA. Cost Study for Manufacturing of Solid Oxide Fuel Cell Power Systems. Richland, WA (United States): 2013. https://doi.org/10.2172/1126362.

[4] Zhao Y, Xia C, Jia L, Wang Z, Li H, Yu J, et al. Recent progress on solid oxide fuel cell: Lowering temperature and utilizing non-hydrogen fuels. Int J Hydrogen Energy 2013;38:16498–517. https://doi.org/10.1016/j.ijhydene.2013.07.077.

[5] Chour K, Chen J, Xu R. Metal-organic vapor deposition of YSZ electrolyte layers for solid oxide fuel cell applications. Thin Solid Films 1997;304:106–12. https://doi.org/10.1016/S0040-6090(97)00017-5.

[6] Gharbage B. Electrical properties of La0.5Sr0.5MnO3 thin films. Solid State Ionics 1995;82:85–94. https://doi.org/10.1016/0167-2738(95)00206-L.

[7] Hayashi K. Sputtered La0.5Sr0.5MnO3–yttria stabilized zirconia composite film electrodes for SOFC. Solid State Ionics 1997;98:49–55. https://doi.org/10.1016/S0167-2738(97)00098-2.

[8] Pal UB. Electrochemical Vapor Deposition of Yttria-Stabilized Zirconia Films. J Electrochem Soc 1990;137:2937. https://doi.org/10.1149/1.2087102.

[9] Irshad M, Siraj K, Raza R, Ali A, Tiwari P, Zhu B, et al. A Brief Description of High Temperature Solid Oxide Fuel Cell's Operation, Materials, Design, Fabrication

Technologies and Performance. Appl Sci 2016;6:75. https://doi.org/10.3390/app6030075.

[10] Fernández-González R, Molina T, Savvin S, Moreno R, Makradi A, Núñez P. Fabrication and electrical characterization of several YSZ tapes for SOFC applications. Ceram Int 2014;40:14253–9. https://doi.org/10.1016/j.ceramint.2014.06.015.

[11] Huang B, Zhu X, Hu W, Wang Y, Yu Q. Characterization of the Ni-ScSZ anode with a LSCM–CeO2 catalyst layer in thin film solid oxide fuel cell running on ethanol fuel. J Power Sources 2010;195:3053–9. https://doi.org/10.1016/j.jpowsour.2009.11.126.

[12] Torabi A, Etsell TH, Sarkar P. Dip coating fabrication process for micro-tubular SOFCs. Solid State Ionics 2011;192:372–5. https://doi.org/10.1016/j.ssi.2010.09.050.

[13] Arendt E, Maione A, Klisinska A, Sanz O, Montes M, Suarez S, et al. Structuration of LaMnO3 perovskite catalysts on ceramic and metallic monoliths: Physico-chemical characterisation and catalytic activity in methane combustion. Appl Catal A Gen 2008;339:1–14. https://doi.org/10.1016/j.apcata.2008.01.016.

[14] da Conceição L, Dessemond L, Djurado E, Muccillo ENS. La0.7Sr0.3MnO3−δ barrier for Cr2O3-forming SOFC interconnect alloy coated by electrostatic spray deposition. Surf Coatings Technol 2014;254:157–66. https://doi.org/10.1016/j.surfcoat.2014.06.005.

[15] Xie H, Su P-C. Fabrication of yttrium-doped barium zirconate thin films with sub-micrometer thickness by a sol–gel spin coating method. Thin Solid Films 2015;584:116–9. https://doi.org/10.1016/j.tsf.2014.11.093.

[16] Steele B. Behaviour of porous cathodes in high temperature fuel cells. Solid State Ionics 1997;94:239–48. https://doi.org/10.1016/S0167-2738(96)00510-3.

[17] Hotza D, Diniz da Costa JC. Fuel cells development and hydrogen production from renewable resources in Brazil. Int J Hydrogen Energy 2008;33:4915–35. https://doi.org/10.1016/j.ijhydene.2008.06.028.

[18] Badwal SPS, Jiang SP, Love J, Nowotny J, Rekas M, Vance ER. A manometric method for the determination of chemical diffusion in perovskite-type cathode materials of the solid oxide fuel cell. Ceram Int 2001;27:431–41. https://doi.org/10.1016/S0272-8842(00)00098-5.

[19] Sahu AK, Ghosh A, Suri AK. Characterization of porous lanthanum strontium manganite (LSM) and development of yttria stabilized zirconia (YSZ) coating. Ceram Int 2009;35:2493–7. https://doi.org/10.1016/j.ceramint.2008.11.012.

[20] Luo X, Yang Y, Yang Y, Tian D, Lu X, Chen Y, et al. Reduced-temperature redox-stable LSM as a novel symmetrical electrode material for SOFCs. Electrochim Acta 2018;260:121–8. https://doi.org/10.1016/j.electacta.2017.11.071.

[21] Darbandi AJ, Enz T, Hahn H. Synthesis and characterization of nanoparticulate films for intermediate temperature solid oxide fuel cells. Solid State Ionics 2009;180:424–30. https://doi.org/10.1016/j.ssi.2009.01.004.

[22] Jiang Y. Electrochemical reduction of oxygen on a strontium doped lanthanum manganite electrode. Solid State Ionics 1998;110:111–9. https://doi.org/10.1016/S0167-2738(98)00111-8.

[23] Haanappel VAC, Mertens J, Rutenbeck D, Tropartz C, Herzhof W, Sebold D, et al. Optimisation of processing and microstructural parameters of LSM cathodes to improve the electrochemical performance of anode-supported SOFCs. J Power Sources 2005;141:216–26. https://doi.org/10.1016/j.jpowsour.2004.09.016.

[24] Carpanese MP, Clematis D, Bertei A, Giuliano A, Sanson A, Mercadelli E, et al. Understanding the electrochemical behaviour of LSM-based SOFC cathodes. Part I — Experimental and electrochemical. Solid State Ionics 2017;301:106–15. https://doi.org/10.1016/j.ssi.2017.01.007.

[25] Bertei A, Carpanese MP, Clematis D, Barbucci A, Bazant MZ, Nicolella C. Understanding the electrochemical behaviour of LSM-based SOFC cathodes. Part II - Mechanistic modelling and physically-based interpretation. Solid State Ionics 2017;303:181–90. https://doi.org/10.1016/j.ssi.2016.09.028.

[26] Seyed-Vakili SV, Babaei A, Ataie M, Heshmati-Manesh S, Abdizadeh H. Enhanced performance of La0.8Sr0.2MnO3 cathode for solid oxide fuel cells by co-infiltration of metal and ceramic precursors. J Alloys Compd 2018;737:433–41. https://doi.org/10.1016/j.jallcom.2017.12.092.

[27] Tarragó DP, Malfatti C de F, de Sousa VC. Obtaining process of ceramic film on substrate by Airbrushed Solution Combustion (ASC) [BR 10 2017 008343 8 A2], 2017.

[28] Florio DZ de, Fonseca FC, Muccillo ENS, Muccillo R. Materiais cerâmicos para células a combustível. Cerâmica 2004;50:275–90. https://doi.org/10.1590/S0366-69132004000400002.

[29] YOKOKAWA H, SAKAI N, KAWADA T, DOKIYA M. Thermodynamic stabilities of perovskite oxides for electrodes and other electrochemical materials. Solid State Ionics 1992;52:43–56. https://doi.org/10.1016/0167-2738(92)90090-C.

[30] Chen RF, Huang Y, Wang CA. Characterization Methods of Pores in Ceramics and Their Analysis. Key Eng Mater 2007;280–283:1819–22. https://doi.org/10.4028/www.scientific.net/KEM.280-283.1819.

[31] Gerstl M, Navickas E, Leitgeb M, Friedbacher G, Kubel F, Fleig J. The grain and grain boundary impedance of sol–gel prepared thin layers of yttria stabilized zirconia (YSZ). Solid State Ionics 2012;225:732–6. https://doi.org/10.1016/j.ssi.2012.02.012.

[32] Gaudon M, Laberty-Robert C, Ansart F, Stevens P, Rousset A. Preparation and characterization of La1–xSrxMnO3+δ (0⩽x⩽0.6) powder by sol–gel processing. Solid State Sci 2002;4:125–33. https://doi.org/10.1016/S1293-2558(01)01208-0.

[33] Cortés-Gil R, Alonso JM, Ruiz-González ML, González-Calbet JM. Topotactic Migration of Cationic Vacancies in La1-tMn1-tO3. Eur J Inorg Chem 2010;2010:3436–40. https://doi.org/10.1002/ejic.201000086.

[34] Tarragó DP, Malfatti C de F, de Sousa VC. Influence of fuel on morphology of

LSM powders obtained by solution combustion synthesis. Powder Technol 2015;269:481–7. https://doi.org/10.1016/j.powtec.2014.09.037.

[35] BRANT M, MATENCIO T, DESSEMOND L, DOMINGUES R. Electrical degradation of porous and dense LSM/YSZ interface. Solid State Ionics 2006;177:915–21. https://doi.org/10.1016/j.ssi.2006.02.012.

[36] Niu Y, Lv W, Chen D, Han J, He W. A model study on correlation between microstructure-gas diffusion and Cr deposition in porous LSM/YSZ cathodes of solid oxide fuel cells. Int J Hydrogen Energy 2019;44:18319–29. https://doi.org/10.1016/j.ijhydene.2019.05.115.

[37] Su C, Lü Z, Wang C, Li J, Li P, Yue X, et al. Effects of a YSZ porous layer between electrolyte and oxygen electrode in solid oxide electrolysis cells on the electrochemical performance and stability. Int J Hydrogen Energy 2019;44:14493–9. https://doi.org/10.1016/j.ijhydene.2019.04.092.

[38] Abdelaziem A, El-Khatib KM, Hafez MA, Badr Y. Effect of annealing on La0.8Sr0.2MnO3 thin films prepared by pulsed laser deposition. Spectrochim Acta Part A Mol Biomol Spectrosc 2019;211:100–7. https://doi.org/10.1016/j.saa.2018.11.060.

[39] Chiba R, Vargas RA, Andreoli M, Seo ESM. Forming of Cathodic Ceramic Film Using Airbrush for Application in High Temperature Solid Oxide Fuel Cells. Mater Sci Forum 2012;727–728:669–74. https://doi.org/10.4028/www.scientific.net/MSF.727-728.669.

[40] Jiang S. A comparison of O2 reduction reactions on porous (La,Sr)MnO3 and (La,Sr)(Co,Fe)O3 electrodes. Solid State Ionics 2002;146:1–22. https://doi.org/10.1016/S0167-2738(01)00997-3.

[41] Das D, Basu RN. Improved polarization behaviour of nanostructured La0.65Sr0.3MnO3 cathode with engineered morphology. Int J Hydrogen Energy 2017;42:15347–58. https://doi.org/10.1016/j.ijhydene.2017.04.254.

[42] Benamira M, Ringuedé A, Cassir M, Horwat D, Pierson JF, Lenormand P, et al. Comparison Between Ultrathin Films of YSZ Deposited at the Solid Oxide Fuel Cell Cathode/Electrolyte Interface by Atomic Layer Deposition, Dip- Coating or Sputtering. Open Fuels Energy Sci J 2009;2:87–99. https://doi.org/10.2174/1876973X01002010087.

[43] Im J, Park I, Shin D. Preparation of nano-crystalline strontium-doped lanthanum manganate (LSM) powder and porous film by aerosol flame deposition. Ceram Int 2014;40:5567–73. https://doi.org/10.1016/j.ceramint.2013.10.148.

[44] Murray EP, Tsai T, Barnett SA. Oxygen transfer processes in (La,Sr)MnO3/Y2O3-stabilized ZrO2 cathodes: an impedance spectroscopy study. Solid State Ionics 1998;110:235–43. https://doi.org/10.1016/S0167-2738(98)00142-8.

[45] Andersson M, Yuan J, Sundn B. SOFC modeling considering electrochemical reactions at the active three phase boundaries. Int J Heat Mass Transf 2012;55:773–88. https://doi.org/10.1016/j.ijheatmasstransfer.2011.10.032.

[46] Ananyev MV, Farlenkov AS, Eremin VA, Kurumchin EK. Degradation kinetics of

LSM–YSZ cathode materials for SOFC. Int J Hydrogen Energy 2018;43:951–9. https://doi.org/10.1016/j.ijhydene.2017.11.107.

[47] Cole KS, Cole RH. Dispersion and Absorption in Dielectrics I. Alternating Current Characteristics. J Chem Phys 1941;9:341–51. https://doi.org/10.1063/1.1750906.

[48] Morales JCR, Vásquez JC, López DM, Martínez JP, Coll DP, Núñez P, et al. Caracterización electroquímica. Pilas Combust. óxidos solidos. 1ª ed., Tenerife: Centro de la Cultura Popular Canaria; 2008, p. 203–42.

[49] Barbucci A, Bozzo R, Cerisola G, Costamagna P. Characterisation of composite SOFC cathodes using electrochemical impedance spectroscopy. Analysis of Pt/YSZ and LSM/YSZ electrodes. Electrochim Acta 2002;47:2183–8. https://doi.org/10.1016/S0013-4686(02)00095-6.

[50] Tarragó DP, Moreno B, Chinarro E, Jurado JR, Malfatti C de F, de Sousa VC. Sintering and electrical properties of strontium- doped lanthanum manganite. Proc. 5th Int. Work. Hydrog. Fuel Cells, Campinas/SP - Brazil: 2010, p. 188–93.

[51] GHOSH A, SAHU A, GULNAR A, SURI A. Synthesis and characterization of lanthanum strontium manganite. Scr Mater 2005;52:1305–9. https://doi.org/10.1016/j.scriptamat.2005.02.020.

[52] Lee H. Electrochemical characteristics of La1−xSrxMnO3 for solid oxide fuel cell. Mater Chem Phys 2003;77:639–46. https://doi.org/10.1016/S0254-0584(02)00091-3.

[53] Yang J, Muroyama H, Matsui T, Eguchi K. A comparative study on polarization behavior of (La,Sr)MnO3 and (La,Sr)CoO3 cathodes for solid oxide fuel cells. Int J Hydrogen Energy 2010;35:10505–12. https://doi.org/10.1016/j.ijhydene.2010.07.174.

[54] Gleiter H. Nanostructured materials: basic concepts and microstructure. Acta Mater 2000;48:1–29. https://doi.org/10.1016/S1359-6454(99)00285-2.

[55] Fan L, Zhu B, Su P-C, He C. Nanomaterials and technologies for low temperature solid oxide fuel cells: Recent advances, challenges and opportunities. Nano Energy 2018;45:148–76. https://doi.org/10.1016/j.nanoen.2017.12.044.

[56] Meng B, Kong M, Yang QQ, Zhang H, Zhu YJ, Lin ZL. Effects of grain-boundary diffusions and modifications on the electrical conductivities of YSZ coatings with columnar microstructure. Solid State Ionics 2014;268:48–53. https://doi.org/10.1016/j.ssi.2014.09.024.

[57] KWON O, CHOI G. Electrical conductivity of thick film YSZ. Solid State Ionics 2006;177:3057–62. https://doi.org/10.1016/j.ssi.2006.07.039.

DEPOSITION OF NANOSTRUCTURED LSM PEROVSKITE THIN FILM ON DENSE YSZ SUBSTRATE BY AIRBRUSHED SOLUTION COMBUSTION (ASC) FOR APPLICATION IN SOFC CATHODES

ABSTRACT

To make SOFC high efficiency energy generation devices, thin ceramic films are proposed as their main components. The rate of the oxygen reduction reaction is relevant for the overall performance of the SOFC, hence a lot of attention is given to the cathodes and their interfaces. The airbrushed solution combustion (ASC) method was used to fabricate an LSM thin film on a dense YSZ substrate. A single phase LSM perovskite was obtained with very thin and interconnected porosity, and a small average grain size (55 nm). The nanostructured LSM thin film electrode showed a low total activation energy (1.27 eV) at high temperatures, but a high area specific resistance at 850°C (55 Ω.cm²). The activation energy for the dissociative adsorption and diffusion of oxygen was significantly low (1.27eV), while the charge transfer and oxygen ion migration activation energy at the LSM/YSZ interface (1.28 eV) was closer to those usually reported.

KEYWORDS: LSM perovskite; nanostructured cathode; SOFC; oxygen reduction reaction; airbrushed solution combustion (ASC).

1. INTRODUCTION

High efficiency energy conversion devices are often referred to as vital for the construction of a sustainable grid based on distributed energy. In this sense, solid oxide fuel cells (SOFC) can play an important role in the near future, due to their great potential as an efficient energy generator, combined with low levels of emissions [1,2]. Nowadays, a few large enterprises already dispose of SOFC systems as their energy supplier, however, substantial use of this technology is yet to come. This is due to the

costs involved in the fabrication and in the maintenance of the SOFC energy banks, which usually requires very specialized labor. Also, their performance and reliability, which are very important commercial factors, are closely related to the fabrication process and component design [3]. In the most recent generation of SOFC devices, the intermediate temperature SOFC (IT-SOFC), the operating temperature is potentially reduced to the range of 500°C to 750°C. The main components are formed by thin films, deposited over each other, in order to form the SOFC stack. The mechanical support of the set is made by the interconnector which, due to the low operating temperature, can be composed of a metallic alloy [4].

Different methods can be used to fabricate thin films for IT-SOFC devices. Techniques based on vapor deposition and those involving the use of plasma, usually allow good microstructure and thickness control of the obtained films and can be conducted using a great variety of materials [5,6]. However, they generally require the use of robust and precise equipment and, in some cases, high processing temperature and expensive raw materials [7,8]. Thin films used in SOFC are also obtained by the processing of ceramic powders. Methods such as tape casting, screen printing, dip coating and spin coating, amongst others, are frequently reported as potential paths for the manufacturing of SOFC devices with low cost equipment and simple technological transfer [9]. The microstructure is controlled by the characteristics of the slurry, which is significantly influenced by the characteristics of the starting powder. Also the use of high sintering temperatures (> 1000°C) is common [10–12]. Precursor solution based methods perform a one-step synthesis and deposition of ceramic materials on the surface of different substrates [13,14]. In such methods, lower processing temperatures can be used and sufficient microstructural control is managed, by selecting suitable experimental conditions [15].

Considering that the cathodic reaction, which is the oxygen adsorption and its reduction and injection in the ion conducting electrolyte, is reported as the limiting factor of the overall SOFC performance, it is important that proper compositional and structural characteristics are achieved through processing [16,17]. Strontium-doped lanthanum manganites (LSM) are the most commonly used materials to compose the cathode in the SOFC. They present chemical and physical compatibility with yttria-stabilized zirconia (YSZ), which is a material generally used as an electrolyte, in typical

operating and processing temperatures of SOFC devices [18,19]. Composite electrodes based on LSM have also been tested for use in cells with YSZ electrolytes [20–22]. A better cathode performance can be achieved when its porous microstructure optimizes the air flow in its interior and, even more important, increases the active sites for the reaction by the enlargement of the triple phase boundary (TPB) zone [23]. Also, the contribution of the gas transport of molecular oxygen to the total cathode polarization is insignificant in thin films with relatively high porosity [24]. More recently, other cathode characteristics such as the length of the adsorption/diffusion process and surface diffusivity of oxygen adsorbed atoms have also been given importance, and they have a close relation with the physical properties and microstructural parameters of the cathode [25]. With the production of a nanostructured component, with small grain and pore size, a decrease in the activation energy may be attained, improving the cathode performance and, consequently, the overall performance of the SOFC device [17,21,26].

In this work, an attempt was made to obtain a LSM thin film with optimum porous microstructure and reduced grain size. The Airbrushed Solution Combustion (ASC) method [27] was tested to fabricate an LSM/YSZ half-cell, by depositing a thin LSM film on a dense YSZ substrate. Structural and morphological characterization of the LSM film was carried out and its electrochemical properties were evaluated in respect to the oxygen reduction reaction mechanism to verify the suitability of the deposition method.

2. EXPERIMENTAL

2.1 Preparation of the half-cell

In order to fabricate the substrate, YSZ powders (Sigma-Aldrich – 99.9%) were mixed in distilled water containing 2.5 wt.% of polyvinyl alcohol (Vetec-Brasil – 99.0%), to act as a binder. After drying for 24 h at 110°C the mixture was sieved using #60 mesh and separated into a portion of 650 mg. It was then submitted to 175 MPa in a uniaxial press using a 12 mm diameter mold. The sintering of the substrate was carried

out in air, using a heating rate of 10°C/min up to a 1450°C plateau, where it was held for 90 min.

A 15 mol% of strontium was chosen as the A-site dopant in the lanthanum manganite thin film, resulting in the $La_{0.85}Sr_{0.15}MnO_3$ compound . Higher Sr ratios are not advisable because it increases the thermal expansion which can make it incompatible with the YSZ substrate [28]. Besides, in amounts up to 15 mol%, Sr^{2+} cations are chemically more stable due to their lower diffusion rate into YSZ electrolytes [29].

The LSM film was deposited on the dense YSZ substrate by the Airbrushed Solution Combustion (ASC) method [27]. The ASC is based on precursor solution techniques with metal salts and organic fuels and with a relatively low processing temperature. In this work, the LSM film was deposited at 650°C and subsequently heat treated at 850°C for 3 hours with a heating and cooling rate of 2°C/min. Further investigations on the ASC deposition of porous ceramic films are being carried out and, also because of patent (BR 10 2017 008343 8 A2) rights, no further details of the deposition step can be given.

2.2 Characterization

The YSZ substrate had its apparent porosity, apparent density and densification determined by the Archimedes method [30]. The rate of densification was calculated considering the mass and volume of the samples and the theoretical density of YSZ as 6.10 g/cm³.

Room temperature X-ray diffraction (XRD) patterns of the YSZ substrates and of the LSM film were collected using a Bruker ASXD8 Advance equipment, in the range (2θ) of 20° to 70° with a 0.05° step and a 2 s capture time. The obtained patterns were compared with the International Centre for Diffraction Data (ICDD) database using the X'pert Highscore tool.

The microstructure of the YSZ substrate, as well as the deposited LSM film, was evaluated with a Hitachi TM-1000 table top scanning electron microscope (TT-SEM). Low magnification micrographs were used to evaluate the YSZ surface and the presence of cracks and continuity of the film. For a more detailed microstructural

observation of the LSM film a Hitachi S-4700 field emission SEM (FEI-SEM) was used. For this analysis the film was initially gold sputtered. After the electrochemical analysis, the half-cell was cold embedded with epoxy resin and cut in half with a diamond disc. The cross sectional observation of the half-cell was carried out in a Zeiss EVO MA10 scanning electron microscope (SEM) with a coupled Energy Dispersive Spectroscope (EDS) detector, and an EDS line scan measurement was performed along the LSM/YSZ interface.

Before the electrochemical impedance spectroscopy (EIS) characterization, the LSM/YSZ half-cell received a sputtered gold cover of a few hundreds of nanometers on both sides, acting as contact electrodes. A Metro-ohm Autolab equipment, internally coupled with a radio frequency analyzer, uses two platinum probes in contact with each side of the gold sputtered faces of the half-cell. Figure 1 shows a scheme of the sample analyzed by EIS. The measurements were done in a furnace, under air atmosphere and at temperatures from 450°C to 850°C, with steps of 50°C and a heating rate of 5°C/min. The frequency range used was from 10^{-2} Hz to 10^{6} Hz, increasing in a logarithmic scale and with AC signal of 50 mV. The collected data was analyzed using the Nova 1.10 software, where the Nyquist plots were fitted and simulated using equivalent circuits, based on electrochemical reaction mechanisms.

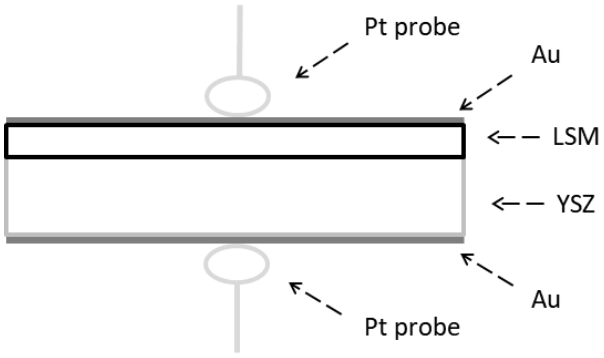

Figure 1: Scheme of the LSM/YSZ half-cell during the EIS analysis.

3. RESULTS AND DISCUSSION

3.1 Phase formation

The sintered YSZ substrate was 1.2 mm thick and 10 mm in diameter. The apparent porosity was determined as 1.44% and the apparent density was 5.99 g/cm³, which compared to the considered theoretical density (6.10 g/cm³), is only 1.8% lower. For this type of substrate a densification of more than 95% is desirable, considering its function as an ion conductor electrolyte and a physical barrier for the separations of gases in the SOFC [28]. The substrate reached a densification of 96.3% and, therefore, attained the required standard for a satisfactory deposition and characterization of the LSM thin film. The densification is slightly lower than the apparent density (98.2%), which may be due to closed pores in the substrate.

In Figure 2.a, an XRD pattern of the obtained YSZ substrate is shown with identified peaks marked. This pattern matched with the ICDD 01-089-9069 file, which corresponds to the cubic structure of zirconium oxide. This phase is the one that shows the higher ionic conductivity and is stabilized at low temperatures by the addition of yttrium oxide [31].

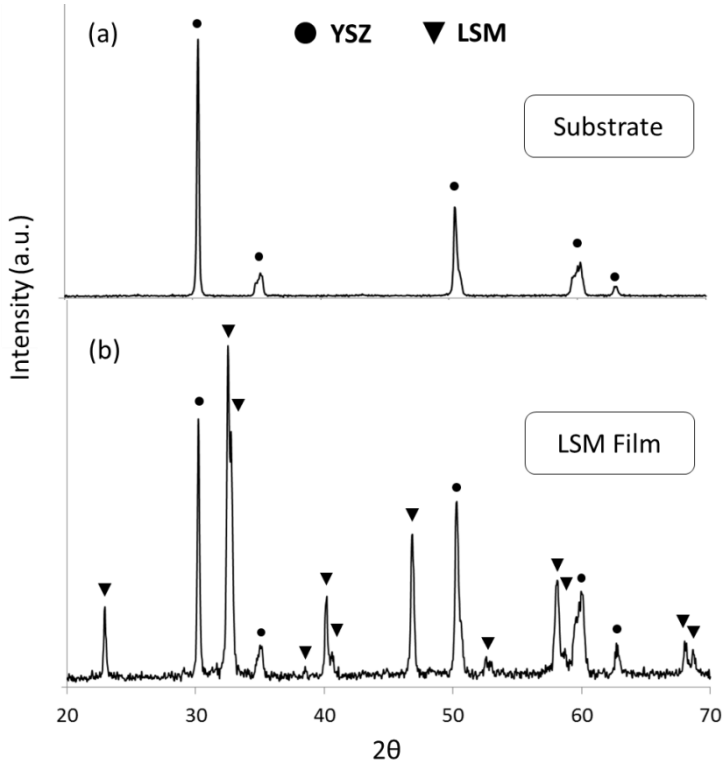

Figure 2: XRD pattern of (a) YSZ substrate and (b) LSM film.

The XRD pattern of the LSM film is shown in Figure 2.b. YSZ peaks are found amongst LSM peaks and are identified with different marks. The LSM film matched file is ICDD 01-089-0648, which corresponds to the rhombohedral perovskite structure. It is known that the addition of bivalent cations, such as Sr^{2+}, in lanthanum manganites induces the formation of Mn^{4+} species. Gaudon et al. [32] studied the influence of dopant concentration on the structure of LSM compositions. It was observed that the concentration of Mn^{4+} ions in the LSM structure is constant for Sr^{2+} amounts of up to 30%. In this composition range, the Mn^{4+} remains at a concentration of around 40% and maintains stable the LSM rhombohedral perovskite structure.

Another important factor is the LSM thermal history. Considering the same strontium amounts (up to 30%), Cortes-Gil et al. verified that when thermally treated below 1000°C, the LSM rhombohedral structure is stable, whereas at higher temperatures the orthorhombic structure is stabilized [33]. In a previous study a heat treatment at 750°C also kept the LSM rhombohedral structure stabilized. Hence, when processing the LSM with such a composition at relatively low temperatures, this structure is more likely to be found [34].

3.2 Morphology

A TT-SEM micrograph of the YZS substrate surface is shown in Figure 3.a. The observed microstructure is composed of sub micrometric grains and the presence of some porosity can also be seen. Despite of these pores, the YSZ substrate microstructure was considered suitable to continue to the film deposition stage, based also on the aforementioned XRD and densification results. The FE-SEM micrograph in Figure 3.b presents a good surface sample of the LSM film deposited on the YSZ substrate. A continuous and porous film is observed. Insignificant remnants of cracks may be seen in the film, which is practically crack free. Gharbage et al. [6] compared an LSM film deposited by ultrasonic spray with an RF sputtered one, both with a final thermal treatment at 900°C, and observed that the first method led to the formation of cracks with sizes between 1 to 10 µm, while with the second method the film structure seemed denser, with few pores.

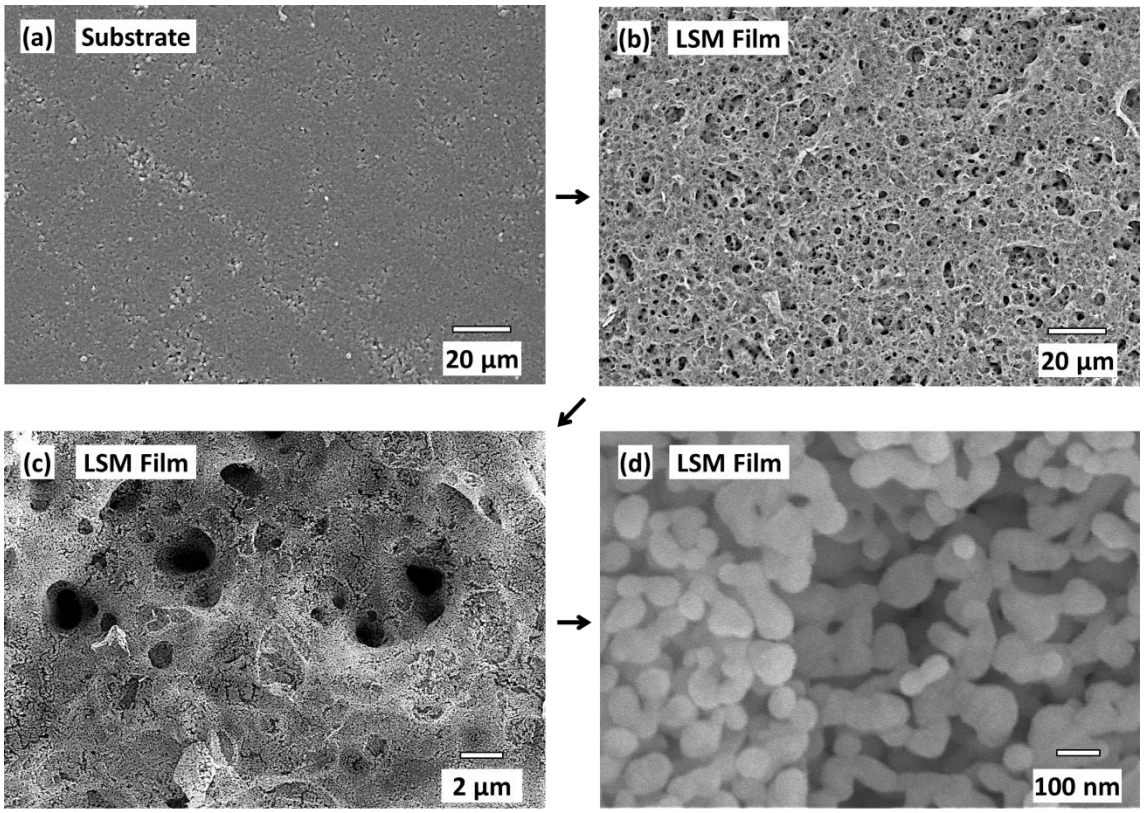

Figure 3: TT-SEM micrograph of the (a) YSZ substrate and FE-SEM micrographs of the (b, c and d) LSM film at different magnifications.

Analyzing the FE-SEM micrographs, shown in Figures 3.c and 3.d, more details are revealed in the microstructure of the LSM film. Regarding the magnification increase in these FE-SEM micrographs, it is assumed that the LSM film obtained by ASC has different structural levels. In Figure 3.c, relatively large pores, with diameters of around 3 µm, are seen and, in a closer look (Figure 3.d), a much finer porosity is revealed. These small pores are very abundant throughout the microstructure and it can be seen that they are intensely interconnected, forming a porosity network. It is assumed that the porous nanostructure obtained by the ASC thin film deposition method can play a very important role in its application as an SOFC cathode, because it can potentially improve the gaseous permeability and impacts on the TPB extension and in the activation energy of the electrochemical reactions [23]. Brant et al. [35] observed that LSM grain growth and coarsening increases the pore size, leading to higher activation energy. Also, Niu et al. [36] observed that pore size distribution influences the current density and lifetime when surface cathode poisoning with foreign ions occurs. Su et al. [37] also mentioned the YSZ surface roughness as an

important factor for the electrochemical performance of LSM, because the formation of wider contact area enhances the TPB zone.

The average grain size of the LSM film obtained by ASC deposition and heat treated at 850°C for 3 hours, is 55 nm. Together with the deposition method and parameters, the temperature applied in the thermal treatment is crucial for the fabrication of nanostructured ceramic films. A minimum temperature is required for better phase crystallization, but an increase in the temperature used can also promote grain growth and, in some cases, may lead to crack formation in the thin film [38]. Table 1 shows the comparison between the processing temperature and method with microstructural features of different LSM films with close compositions. The use of an airbrush was tested by Chiba et al. [39] for the deposition of a LSM suspension on an YSZ electrolyte and the films was heat treated at 1200°C and reached a final thickness of 30 µm. Hayashi et al. [7] deposited LSM cathode compositions using radio-frequency sputtering and verified grain growth in the film from 20 nm to 150 nm, because of the need of a 1000°C heat treatment. It was also reported that after the heat treatment, the grain morphology was square-shaped. The use of powder processing methods tends to promote even more significant grain growth, because they require higher processing temperatures. The screen printing deposition of LSM powders obtained by co-precipitation, as performed by Jiang [40], resulted in a 360 nm average grain size when a 1150°C heat treatment was used. The same method was used by Das et al. [41], but the final thermal treatment was at 1000°C, and it was observed that the size of the grains was mostly submicrometric with some larger grains of 1 to 2 µm. Benamira et al. [42] tested a simple brush painting of a commercial submicrometric LSM slurry, followed by sintering at 1200°C, where the average grain size seems to be smaller than 500 nm. A similar procedure was followed by Seyed-Vakili et al. [26] that used an even lower sintering temperature (1100°C) but ended up with larger grains. On the other hand, this same temperature used by Brant et al. [35] to treat commercial LSM powder deposited through a painting process, resulted in an average grain size of 200 nm. The aerosol flame deposition performed by Im et al. [43] also needed a thermal treatment of 1200°C and produced an even larger grain growth, close to 800 nm. Darbandi et al. [21] performed a spin coating deposition of LSM powder with particles measuring from 20 to 50 nm and, after a low temperature

thermal treatment (850°C), the final grain size did not seem to have varied much, with an average size being close to 100 nm.

Table 1: Cathodic material, deposition method, processing temperature and microstructural features of LSM films found in the literature among with the one obtained by ASC.

Ref. n°	Cathodic material	Deposition method	Process temperature	Grain size (nm)	Thickness (µm)
*	$La_{0.85}Sr_{0.15}MnO_3$	ASC	850°C	55	10
[6]	$La_{0.5}Sr_{0.5}MnO_3$	RF sputtering	900°C	NA	1
[6]	$La_{0.5}Sr_{0.5}MnO_3$	ultrasonic spray	900°C	NA	10
[7]	$La_{0.5}Sr_{0.5}MnO_3$	RF sputtering	1000°C	150	0.6 – 1.2
[21]	$La_{0.75}Sr_{0.2}MnO_{3-\delta}$ [n]	spin coating	850°C	< 100 #	0.5
[21]	$(La_{0.8}Sr_{0.2})_{0.95}MnO3_{-\delta}$ [µ]	screen printing	1150°C	NA	10
[26]	$La_{0.8}Sr_{0.2}MnO_3$	painting	1100°C	~ 1000 #	40
[22]	$La_{0.8}Sr_{0.2}MnO_3$/20%YSZ	screen printing	1200°C	NA	35
[35]	$La_{0.65}Sr_{0.35}MnO_3$	painting	1100°C	200	NA
[39]	$La_{0.85}Sr_{0.15}MnO_3$	airbrushing	1200°C	NA	30
[40]	$La_{0.72}Sr_{0.18}MnO_3$	screen printing	1150°C	360	50
[41]	$La_{0.65}Sr_{0.3}MnO_3$	screen printing	1000°C	~ 1000 #	50
[42]	$La_{0.8}Sr_{0.2}MnO_3$	painting	1200°C	< 500 #	12
[43]	$La_{0.8}Sr_{0.2}MnO_3$	aerosol flame	1200°C	< 800 #	8
[44]	$La_{0.8}Sr_{0.2}MnO_3$	spin coating	1100°C	NA	10

** this work NA not available # estimated from micrographs*

The cross sectional SEM micrograph taken at the end of the experimental procedure, is displayed in Figure 4.a. The thickness of the LSM film is 10 µm and, amongst the fine porosity discussed above, flattened larger pores were observed. Also, the porous LSM film looks well adhered to the YSZ substrate. In general, the techniques used for LSM deposition are versatile with respect to film thickness, as depicted in Table 1. Usually, sputtering methods allow the production of thinner films, of around a few micrometers or even less [6,7]. Through powder processing methods of LSM, or LSM/YSZ composites, it is more common to find thicknesses of a few dozen

micrometers [22,26,40,41]. Nevertheless, films with reduced thickness can also be achieved by conventional powder processing, as demonstrated by the brush painting and the spin coating performed by Benamira et al. [42] and Murray et al. [44], where the produced films were 12 and 10 µm thick, respectively. In some cases, ultrathin LSM films can be obtained by conventional powder processes, like the spin coating performed by Darbandi et al. [21], which resulted in a 0.5 µm thick film. Methods based on wet chemistry are also used in the production of thin LSM films. Gharbage et al. [6] used ultrasonic spray deposition and obtained a 10 µm thick LSM film, and Im et al. [43] reached 8 µm in a LSM film deposited by aerosol flame deposition. An study accomplished by Andersson et al. [45], using numeric modelling, demonstrated that 90% of the electrochemical reactions occur within a distance of 10 µm from the electrode/electrolyte interface and that thicker components may only increase ohmic losses. Also, Carpanese et al. [24] demonstrated that the polarization due to O_2 diffusivity is some orders of magnitude lower that the total cathode polarization in films as thin as 3 µm. The material costs also depend on the film thickness and can be reduced along with it. Hence, it is advisable that cathode thickness is less, or not much more, than 10 µm. In this sense, compared with data shown in Table 1, the LSM film thickness obtained by ASC deposition was considered suitable.

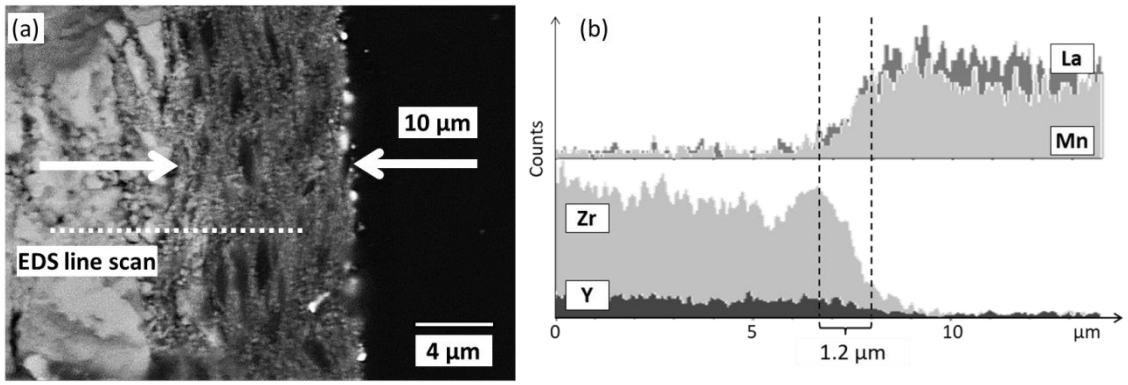

Figure 4: (a) Cross sectional SEM micrograph of the LSM thin film and (b) EDS line scan profile for the major elements.

In Figure 4.b the EDS line scan result is shown. The variation of the relative amounts of the main components of the substrate and the film were measured. Analyzing the elemental profile obtained from the YSZ substrate side, a high concentration of Zr in contrast with Y is observed, as expected. In the LSM film side,

the concentrations of La and Mn are similar. Considering the highest peaks of Zr, La and Mn near the interface it, was possible to determine a gradual transition of elements with a width of 1.2 μm. This may represent a region with more intense electrochemical activity or, less likely, due to the low heat treatment temperature (850°C), a dielectric phase formation process. Ananyev et al. [46] studied the cation interdiffusion in LSM/YSZ composite cathodes and observed a much smaller width of variable composition. It was determined that at high temperature exposure, this transient area tends to grow with time.

3.3 Electrochemical characterization

The measurements performed by the EIS technique can be used to determine the activity of catalysts in terms of an interfacial polarization resistance of a solid electrode/electrolyte interface. Such a relation occurs due to the similarity of the electrochemical behavior with an electrical circuit formed, essentially, by resistive and capacitive elements and, in some cases, inductive elements also. This implies that each electrochemical phenomenon presents a conservative element, independent of the frequency, in addition to the dissipative one. In this sense, the relative capacitance of a constant phase element can indicate the nature of an electrochemical phenomenon associated with a determined resistance [47,48]. Usually, the response of an LSM porous film deposited on an YSZ substrate is considered as two semi-circles in the Nyquist plot. The influence of temperature and microstructure at atmospheric pressure (pO_2 = 0.21 atm) on the overall cathode behavior was analyzed considering the separate influence of each phenomenon represented by a semi-circle in the impedance spectrum.

Figure 5.a shows the EIS spectra of the LSM/YSZ half-cell obtained at 550°C and 600°C. For the resistance values of both axes in the Nyquist plot, the area of the contact electrode was considered such that all the results are shown in terms of area specific resistance (ASR) and are designated solely with the letter R. In all measured temperatures up to 550°C, a small arc is observed in the high frequency region, followed by a larger arc composed by two overlapping semi-circles. At temperatures of 600°C and above, only the larger arc is observed. For this reason, the equivalent circuit

used to fit the experimental data for the spectra obtained at temperatures up to 550°C, is different from those obtained at temperatures of 600°C and above. At lower temperatures (T < 550°C), the equivalent circuit is composed of a serial resistance Rs connected to three RQ systems, where each RQ is a resistance R in parallel with a constant phase element Q. However, at higher temperatures (T > 600°C) there are only two RQ systems connected to Rs, as illustrated in Figure 5.b.

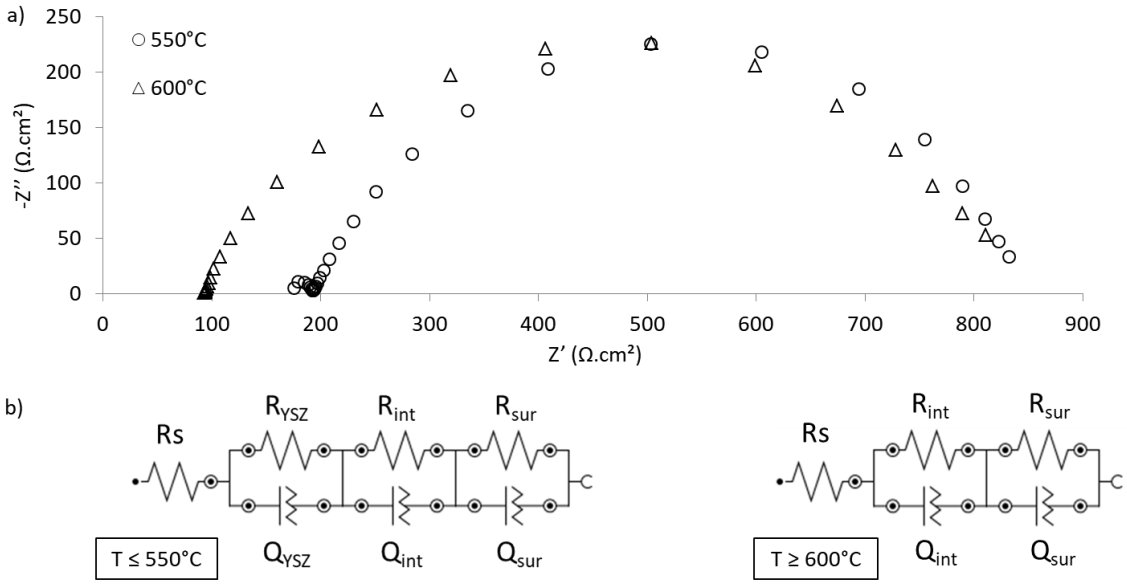

Figure 5: (a) Impedance experimental data at 550°C and 600°C and (b) equivalent circuits for different temperatures.

As 550°C is considered a relatively low temperature, besides the serial resistance (Rs), the high frequency RQ system can also be attributed to an electrolytic process and is represented as $(RQ)_{YSZ}$. The Q_{YSZ} element of the half-cell studied presented a capacitance value in the order of 10^{-9} F/cm². This value is within a range of capacitance associated with grain boundary processes suggesting that R_{YSZ} corresponds to the oxygen ion conduction resistance in the grain boundary of the YSZ electrolyte. Therefore, the Rs resistance in such temperatures represents the resistance inside the YSZ electrolyte grains [31,48]. This same behavior where the high frequency arc tends to lose its capacitive element with increasing temperature, has been reported in the literature [40,43]. The temperature where the $(RQ)_{YSZ}$ disappears depends, mainly, on the properties of the electrolyte and it can vary from under 600°C to temperatures just

above 700°C. In this process, the R_{YSZ} becomes part of the Rs and, at high temperatures, the Rs corresponds to the total ohmic resistance of the YSZ electrolyte.

The larger arc is associated with electrode processes and can be decomposed into two overlapped semi-circles, as reported by different authors [21,22,35,40,42,43]. Running the simulation of the obtained data considering two RQ systems in the half-cell, a capacitance in the order of 10^{-4} F/cm² is found in the lower frequency arc. This value indicates electrochemical reactions. In this case, it is attributed to the reactions and diffusion on the LSM surface, corresponding to the $(RQ)_{sur}$ elements. The other arc considered at intermediate frequencies has a capacitance in the order of 10^{-5} F/cm², which is a typical value for an interface process. It is related to the cathode/electrolyte charge transfer from the LSM films to the YSZ [40,43,48]. The interface elements are called $(RQ)_{int}$.

The reaction mechanism adopted by different authors assumes that four steps can take place in the LSM/YSZ half-cell. At first, the gaseous O_2 penetrates the porous LSM structure and is adsorbed in a favorable site on the LSM surface (O_{ads}). The adsorption promotes the O_2 molecule dissociation, using electrons from the external circuit. The dissociated O^- diffuses on the TPB area and proximities, towards the YSZ electrolyte. Once it finds an oxygen vacancy in the YSZ lattice, it undergoes the complete reduction to O^{2-} and it is fully incorporated in the electrolyte. For a better understanding of the relationship between the reaction mechanisms, the data generated by the impedance spectrum, and the fit and simulation treatment with equivalent circuits, a schematic illustration is shown in Figure 6. The dots are the experimental results obtained at 550°C, and the full line connecting them is the simulation result obtained with the software. Drawn below this curve are the semi-circles considered for the fit and simulation. In this model, the RQ elements of the electrode, $(RQ)_{int}$ and $(RQ)_{sur}$, can represent more than one reaction step, if compared to the mechanism described earlier. The resistance R_{sur} is associated with the dissociative adsorption of oxygen and diffusion, while the R_{int} resistance is related to the complete reduction of oxygen and injection in the YSZ electrolyte lattice.

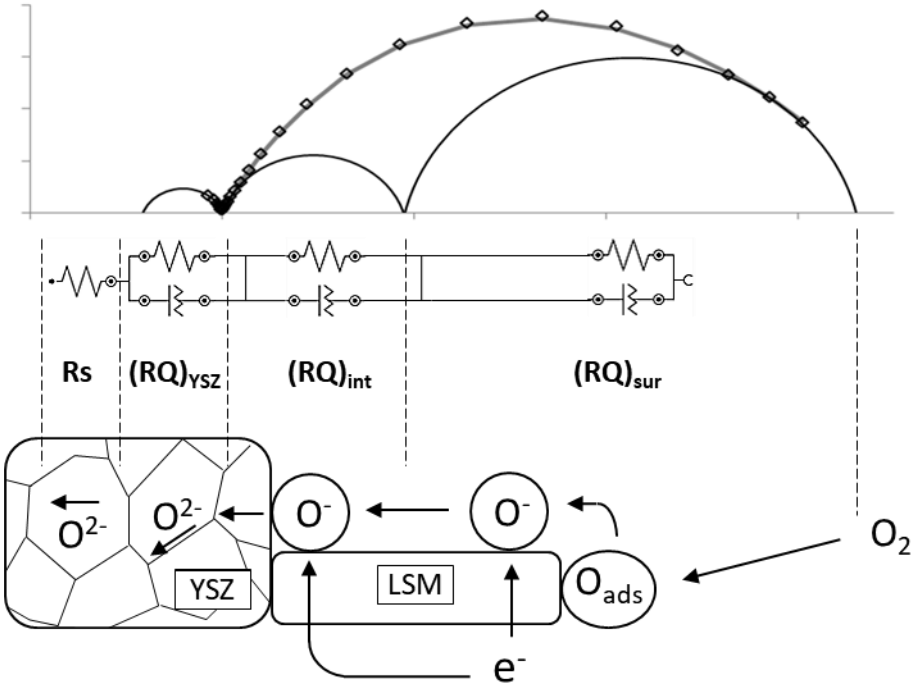

Figure 6: Scheme of the relationship between the impedance spectrum, the equivalent circuits, and the electrochemical reaction mechanism of oxygen reduction in the LSM/YSZ interface and nearby.

Figure 7 shows the Arrhenius plot of the overall electrode area specific resistance (R_e), which is the sum of R_{sur} and R_{int}, and represents to total charge transfer polarization of the electrode process [21,41]. A change in the curve slope is observed and starts at 550°C, where R_e remains virtually constant until 650°C. From this temperature on, the decrease in R_e occurs with different behavior, which means that there is a variation in the total activation energy of the electrode (Ea_e). At lower temperatures (T < 550°C) the Ea_e is 1.05 eV, and above 650°C, it is increased to 1.27 eV. As the oxygen reduction in the LSM/YSZ pair occurs through various reaction steps, this change can be attributed to a shift in the rate determining step of the overall reaction. Jiang et al. [22] stated that a theoretical variation in anodic and cathodic charge transfer coefficient can occur at a temperature around 700°C. The author attributed this deviation to the rate determining step shift and demonstrated experimentally the temperature influence on the Ea_e of LSM/YSZ composite cathodes, obtaining 1.33 eV at lower temperatures (T < 700°C), and 1.59 eV at elevated temperatures, above 700°C. Benamira et al. [42] observed a similar variation in the Ea_e of pure LSM cathode, where a deviation of Ea_e from 1.00 eV, up to 480°C, to 1.92 eV at

higher temperatures (T > 510°C), was observed. It is noted that the shift of the rate determining step can take place at a range of temperatures, with different shift temperatures being found in the literature. The starting temperature (550°C) and the Ea_e at low temperatures (1.05 eV) are close to those reported by Benamira et al. [42]. While at higher temperatures (T > 650°C) the obtained value of Ea_e (1.27 eV) and the electrode behavior change temperature are nearest to those reported by Jiang et al. [22]. Barbucci et al. [49] observed that the addition of YSZ to the LSM cathode only influenced the polarization resistance, and did not influence the activation energy, where an Ea_e of around 1.04 eV (T > 700°C) was verified for pure LSM and for cathodes with different amounts of YSZ. This statement corroborates an earlier study carried out by Murray et al. [44], where it is also inferred that the presence of YSZ in the LSM electrode does not change the rate determining step and, consequently, does not change the Ea_e. Nevertheless, they reported a slight decrease in the Ea_e from 1.61 eV for pure LSM, to 1.49 eV for LSM/50%YSZ composite. The possibility of the shift in the Ea_e have been caused by grain growth or microstructural modifications was discharged, since it is reported to occur only at temperatures above 1000°C, even for powders with reduced grain size [50,51].

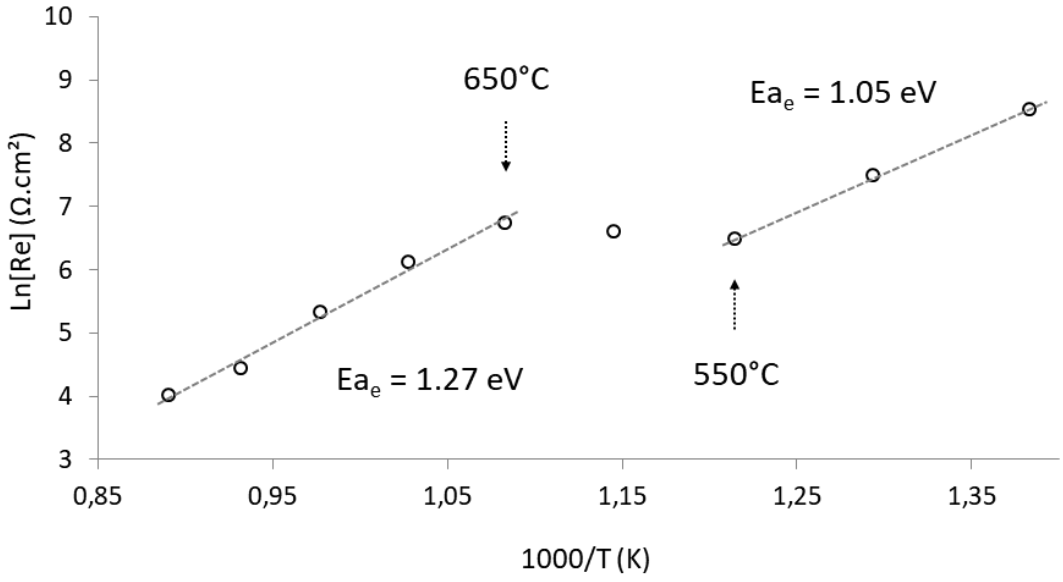

Figure 7: Variation of the overall electrode resistance (R_e) of the LSM thin film with temperature.

Table 2 brings together the electrochemical characteristics of the LSM electrode deposited by the ASC process with other results reported by different authors with various cathode compositions. Values of Ea_e at high temperatures, near 2.00 eV, can be found in the literature as well as values closer to 1.00 eV. This is because many variables can influence the total Ea_e, like the morphological aspects, the actual composition of the LSM thin films, adherence and contact with the YSZ substrate, and also its electrolytic characteristics. Although some authors correlate the LSM thin film microstructure with the activation energy and total polarization, in the studies referred to this work, a direct and general correlation of these factors is not easily observed due to divergence or lack of information. Lee [52] screen printed an $La_{0.5}Sr_{0.5}MnO_3$ thin film on an YSZ substrate and obtained an Ea_e of 1.76 eV (T > 600°C) with a firing temperature of 1100°C. Yang et al. [53] used the same method, with a firing temperature of 1150°C, to deposit a $(La_{0.8}Sr_{0.2})_{o.97}MnO_3$ thin film and found a similar Ea_e value of 1.80 eV (T > 800°C). When the substrate was changed to samarium-doped ceria, the Ea_e decreased to 1.47 eV, highlighting the influence of the electrolyte on the overall electrode activation energy (Ea_e). The influence of annealing temperature of $La_{0.65}Sr_{0.35}MnO_3$ thin films was reported by Brant et al. [35]. When fired in temperatures up to 1200°C, the Ea_e obtained was near 1.20 eV, and above these temperatures a gradual increase was observed, attributed to the loss of porosity of the thin film and also to the formation of secondary phases in the LSM/YSZ interface, with the Ea_e reaching up to 2.00 eV. Compared with these works, the high temperature Ea_e of the LSM thin film deposited by ASC (1.27 eV, T > 650°C) can be considered low and it is likely that this fact is related to the influence of the morphological characteristics of the thin film, such as small grain size and fine interconnected porosity. Darbandi et al. [21] compared LSM cathodes obtained from commercial micro LSM powder with a synthesized nanopowder and reported a reduction in the Ea_e from 1.52 to 1.41 eV (T > 500°C). For a similar commercial LSM starting powder, Seyed-Vakili et al. [26] obtained the same value of Ea_e (1.52 eV), whereas the film was sintered at 1150°C, which is 50°C higher.

Table 2: Electrochemical properties of LSM thin film deposited by ASC, amongst those reported by different authors.

Ref. n°	Cathodic material	Temp. range	Ea_e (eV)	Ea_{int} (eV)	Ea_{sur} (eV)	ASR-850°C (Ω.cm²)
*	$La_{0.85}Sr_{0.15}MnO_3$	< 550°C	1.05	0.86	1.37	NA
*	$La_{0.85}Sr_{0.15}MnO_3$	> 650°C	1.27	1.28	1.27	55
[21]	$La_{0.75}Sr_{0.2}MnO_{3-\delta}$ n	> 500°C	1.41	NA	NA	0.62
[21]	$(La_{0.8}Sr_{0.2})_{0.95}MnO_3$ μ	> 500°C	1.52	NA	NA	2.32
[21]	$La_{0.75}Sr_{0.2}MnO_{3-\delta}$/25%GDC	> 500°C	1.13	NA	NA	0.06
[26]	$La_{0.8}Sr_{0.2}MnO_3$	> 600°C	1.52	NA	NA	6.71 [-]
[35]	$La_{0.65}Sr_{0.35}MnO_3$	> 900°C	1.20-2.00	NA	NA	NA
[37]	$(La_{0.75}Sr_{0.25})_{0.95}MnO_{3-\delta}$	800°C	NA	NA	NA	7.59 [-]
[40]	$La_{0.72}Sr_{0.18}MnO_3$	> 700°C	2.22	1.13	3.04	6.2 [+]
[42]	$La_{0.8}Sr_{0.2}MnO_3$	< 500°C	1.00	NA	NA	NA
[42]	$La_{0.8}Sr_{0.2}MnO_3$	> 500°C	1.92	NA	NA	NA
[43]	$La_{0.8}Sr_{0.2}MnO_3$	> 600°C	1.48	1.60	1.38	1.7 [+]
[22]	$La_{0.8}Sr_{0.2}MnO_3$ / 20% YSZ	< 700°C	1.33	NA	NA	NA
[22]	$La_{0.8}Sr_{0.2}MnO_3$ / 20% YSZ	> 700°C	1.59	NA	NA	12 [#]
[44]	$La_{0.8}Sr_{0.2}MnO_3$	> 550°C	1.61	NA	NA	0.70 [#]
[44]	$La_{0.8}Sr_{0.2}MnO_3$ / 50% YSZ	> 550°C	1.49	NA	NA	0.09 [#]
[49]	$(La_{0.75}Sr_{0.25})_{0.95}MnO_{3\ddagger\delta}$	> 700°C	1.04	NA	NA	4.5 [#]
[52]	$La_{0.5}Sr_{0.5}MnO_3$	> 600°C	1.76	NA	NA	7.9 [#]
[53]	$(La_{0.8}Sr_{0.2})_{0.97}MnO_3$	> 800°C	1.80	NA	NA	3.8 [#]

** this work NA not available [#] estimated from Arrhenius plot [-]800°C [+]900°C*

A comparison between R_{int} and R_{sur} behavior with increasing temperature is shown in the Arrhenius plot of Figure 8. A change in the predominant behavior, together with a shift in the E_a of both reactions, is noted. At low temperatures (T < 550°C) the LSM/YSZ interface reaction is predominant, showing a higher ASR (R_{int}), while at higher temperatures (T > 650°C) the ASR of the LSM surface reaction (R_{sur}) has higher values. Im et al. [43] observed a similar transition of the predominant reaction occurring at slightly higher temperatures, in the range of 650°C to 750°C, assuming that R_{int} is related to the charge transfer resistance in the LSM/YSZ interface and R_{sur} to

the dissociative adsorption and diffusion of oxygen in the LSM surface. On the other hand, Jiang [40] reported a different behavior, where R_{sur} is predominant at lower temperatures while R_{int} has higher ASR values at higher temperatures, with the transition occurring around 800°C.

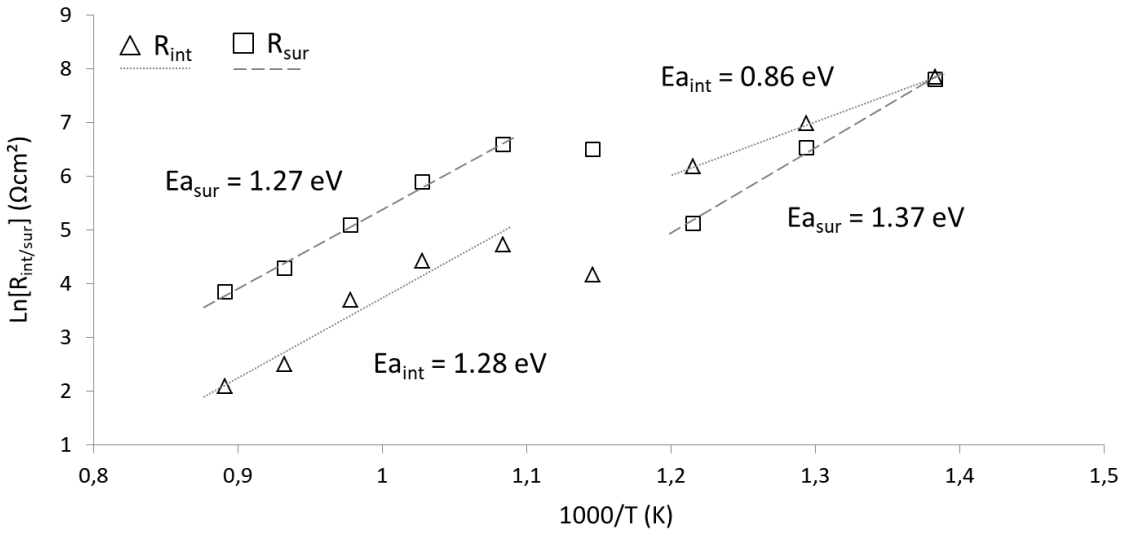

Figure 8: Arrhenius plot of Ri_{nt} and R_{sur}.

The activation energy of the LSM/YSZ interface (Ea_{int}) at temperatures lower than 600°C is 0.86 eV, and at higher temperatures increased to 1.28 eV. At the interface, charge transfer and oxygen ion migration take place. It is possible that a variation in the predominant step at R_{int} occurs from low to high temperatures [22,40,42]. Considering the E_{aint} at higher temperatures (1.28 eV), the obtained value is between the 1.13 eV, reported by Jiang [40], and the 1.60 eV obtained by Im et al. [43]. The activation energy of the LSM surface (Ea_{sur}) decreased from 1.37 eV to 1.28 eV with rising temperature. In this region, the dissociative adsorption and diffusion of oxygen are the considered steps [22,40,42] and, again, the temperature seems to influence the predominant one. At higher temperatures, the Ea_{sur} (1.27 eV) is lower than those in literature [40,43].

Considering the values of Ea_{int} and Ea_{sur} obtained at high temperatures and the microstructure observed in this study, compared with other works, it may be inferred that a thicker film, such as the one obtained by Jiang [40] with 50 µm, results in a higher value of Ea_{sur} (3.04 eV), while thinner films may cause a decrease in Ea_{sur}, as

seen in the report of Im et al. [43] (1.38 eV) with a thickness of 8 µm, and in this work where with a 10 µm thick film, an Ea_{sur} of 1.27 eV was achieved. The small grain size and fine interconnected porosity of the LSM film deposited by ASC may have influenced the relatively low Ea_{sur} obtained. These morphological aspects can also be related to low Ea_{int}. The Ea_{int} and average grain size of Jiang [40], and Im et al. [43], were 1.13 eV for 360 nm and 1.60 eV for 1 µm, respectively. In this work, an Ea_{int} of 1.28 eV was obtained for an average grain size of 55 nm and it is possible that these values could be lowered by improving the substrate quality and interface adhesion, as discussed below.

The total electrode ASR (R_e) is strongly influenced by measurement temperature and can undergo other variations due to structural characteristics, such as grain size, porosity, thickness and substrate material [21,26,35]. The R_e at 850°C obtained in this study (55 Ω.cm²) is relatively high when compared to results reported by other authors. Usually, R_e values remain under 10 Ω.cm², as shown in Table 2. Lee [52] and Yang et al. [53] screen printed LSM compositions with sintering temperatures of 1100°C and 1150°C and reported 7.9 Ω.cm² and 3.8 Ω.cm² at 850°C, respectively, which are already relatively high values. At the temperature of 900°C, Jiang [40] and Im et al. [43] reported R_e as 6.2 Ω.cm² and 1.7 Ω.cm², respectively. Lower ASR values can be achieved with the use of composite cathodes, such as in the works of Murray et al. [44], which tested LSM with 50% of YSZ and obtained 0.09 Ω.cm², and Darbandi et al. [21], which used LSM with 25% gadolinium-doped ceria and reached 0.06 Ω.cm². Barbucci et al. [49] observed that the addition of up to 50% YSZ to LSM cathodes decreased the ASR values, whereas, at higher concentrations the ASR showed an increase. The study with YSZ buffer layers, by Benamira et al. [42], indicates that the contact quality between components could directly influence the total electrode ASR. The use of a YSZ porous interlayer could also lead to better and broader LSM/YSZ interface contact, according to the study of Su et al. [37], where the use of such a layer decreased the total polarization resistance from 7.59 Ω.cm² to 2.19 Ω.cm², at 800°C. At this same temperature, Sayed-Vakili et al. [26] obtained 6.71 Ω.cm² by testing a commercial LSM material. Somehow, even with improved morphological characteristics and low values of Ea_e, the LSM film obtained by ASC presented high polarization resistance.

Considering the LSM nanostructure it was expected a decrease in both Ea_e and R_e. It is known that nanocrystalline materials can present a change in the energetic state of interfaces, including gas/solid and solid/solid interfaces [54,55]. This change in the interface energy can explain the promising Ea_e values reported in this work, since the activation energies depend directly on the surface energetic state. On the other hand, nanostructures also provide an increase in the active sites and defects concentration, as well as enhancement in thin films adherence and, consequently, a decrease in Re should have been observed [41,55], but in despite of it a high R_e value was found. It is possible that microstructural defects within the YSZ bulk have caused deleterious effects on the cathode performance, since it was already reported that nature and quality of the electrolyte can directly influence the cathode polarization;

The YSZ electrolyte is a pure ionic conductor and, in this work, the total conductivity of the electrolyte was found higher (0.048 S/cm) than the usually reported [56,57]. Kwon and Choi [57] reported that the difference between the conductivity of YSZ bulk and thin film is observed only when an across-plane current is tested, while in an in-plane current the conductivities are alike. In this sense, the lamination like defects observed in the electrolyte in Figure 4.a may be the cause of poor electrolyte conductivity and, consequently, high R_e of the LSM film.

4. CONCLUSIONS

A porous 10 µm thick nanostructured LSM film was deposited on a dense YSZ substrate by the ASC method. The film presented no secondary phases, being composed of crystalline LSM rhombohedral perovskite after heat treatment. Enhanced morphological characteristics were observed, such as very fine and interconnected porosity and an average grain size of 55 nm. The activation energy of the electrode, as well as the LSM/YSZ interface and LSM surface activation energies underwent an increase at temperatures higher than 650°C, but still remained low compared to the literature values, probably due to the morphological characteristics. The total electrode ASR (55 $\Omega.cm^2$) was considered high for the LSM/YSZ system, probably due to microstructural defects in the YSZ electrolyte that decreased its conductivity and,

hence, the cathode global performance. The development of nanostructured thin ceramic films using the ASC method is promising and further investigation must be carried out for optimum use of this novel deposition technique.

5. ACKNOWLEDGEMENTS

The authors would like to thank *Conselho Nacional de Desenvolvimento Científico e Tecnológico* (CNpQ) and *Coordenação de Aperfeiçoamento de Pessoal de Nível Superior* (CAPES) in Brazil and *Instituto de Cerámica y Vidrio* (ICV) and *Consejo Superior de Investigaciones Científicas* (CSIC) in Spain. Also, especial thanks to Dr. José Ramón Jurado who helped with the lead of our group in this research.

6. REFERENCES

[1] Stambouli AB, Traversa E. Solid oxide fuel cells (SOFCs): a review of an environmentally clean and efficient source of energy. Renew Sustain Energy Rev 2002;6:433–55. https://doi.org/10.1016/S1364-0321(02)00014-X.

[2] Omer AM. Green energies and the environment. Renew Sustain Energy Rev 2008;12:1789–821. https://doi.org/10.1016/j.rser.2006.05.009.

[3] Weimar MR, Chick LA, Gotthold DW, Whyatt GA. Cost Study for Manufacturing of Solid Oxide Fuel Cell Power Systems. Richland, WA (United States): 2013. https://doi.org/10.2172/1126362.

[4] Zhao Y, Xia C, Jia L, Wang Z, Li H, Yu J, et al. Recent progress on solid oxide fuel cell: Lowering temperature and utilizing non-hydrogen fuels. Int J Hydrogen Energy 2013;38:16498–517. https://doi.org/10.1016/j.ijhydene.2013.07.077.

[5] Chour K, Chen J, Xu R. Metal-organic vapor deposition of YSZ electrolyte layers for solid oxide fuel cell applications. Thin Solid Films 1997;304:106–12. https://doi.org/10.1016/S0040-6090(97)00017-5.

[6] Gharbage B. Electrical properties of La0.5Sr0.5MnO3 thin films. Solid State Ionics 1995;82:85–94. https://doi.org/10.1016/0167-2738(95)00206-L.

[7] Hayashi K. Sputtered La0.5Sr0.5MnO3–yttria stabilized zirconia composite film electrodes for SOFC. Solid State Ionics 1997;98:49–55. https://doi.org/10.1016/S0167-2738(97)00098-2.

[8] Pal UB. Electrochemical Vapor Deposition of Yttria-Stabilized Zirconia Films. J Electrochem Soc 1990;137:2937. https://doi.org/10.1149/1.2087102.

[9] Irshad M, Siraj K, Raza R, Ali A, Tiwari P, Zhu B, et al. A Brief Description of High Temperature Solid Oxide Fuel Cell's Operation, Materials, Design, Fabrication

Technologies and Performance. Appl Sci 2016;6:75. https://doi.org/10.3390/app6030075.

[10] Fernández-González R, Molina T, Savvin S, Moreno R, Makradi A, Núñez P. Fabrication and electrical characterization of several YSZ tapes for SOFC applications. Ceram Int 2014;40:14253–9. https://doi.org/10.1016/j.ceramint.2014.06.015.

[11] Huang B, Zhu X, Hu W, Wang Y, Yu Q. Characterization of the Ni-ScSZ anode with a LSCM–CeO2 catalyst layer in thin film solid oxide fuel cell running on ethanol fuel. J Power Sources 2010;195:3053–9. https://doi.org/10.1016/j.jpowsour.2009.11.126.

[12] Torabi A, Etsell TH, Sarkar P. Dip coating fabrication process for micro-tubular SOFCs. Solid State Ionics 2011;192:372–5. https://doi.org/10.1016/j.ssi.2010.09.050.

[13] Arendt E, Maione A, Klisinska A, Sanz O, Montes M, Suarez S, et al. Structuration of LaMnO3 perovskite catalysts on ceramic and metallic monoliths: Physico-chemical characterisation and catalytic activity in methane combustion. Appl Catal A Gen 2008;339:1–14. https://doi.org/10.1016/j.apcata.2008.01.016.

[14] da Conceição L, Dessemond L, Djurado E, Muccillo ENS. La0.7Sr0.3MnO3−δ barrier for Cr2O3-forming SOFC interconnect alloy coated by electrostatic spray deposition. Surf Coatings Technol 2014;254:157–66. https://doi.org/10.1016/j.surfcoat.2014.06.005.

[15] Xie H, Su P-C. Fabrication of yttrium-doped barium zirconate thin films with sub-micrometer thickness by a sol–gel spin coating method. Thin Solid Films 2015;584:116–9. https://doi.org/10.1016/j.tsf.2014.11.093.

[16] Steele B. Behaviour of porous cathodes in high temperature fuel cells. Solid State Ionics 1997;94:239–48. https://doi.org/10.1016/S0167-2738(96)00510-3.

[17] Hotza D, Diniz da Costa JC. Fuel cells development and hydrogen production from renewable resources in Brazil. Int J Hydrogen Energy 2008;33:4915–35. https://doi.org/10.1016/j.ijhydene.2008.06.028.

[18] Badwal SPS, Jiang SP, Love J, Nowotny J, Rekas M, Vance ER. A manometric method for the determination of chemical diffusion in perovskite-type cathode materials of the solid oxide fuel cell. Ceram Int 2001;27:431–41. https://doi.org/10.1016/S0272-8842(00)00098-5.

[19] Sahu AK, Ghosh A, Suri AK. Characterization of porous lanthanum strontium manganite (LSM) and development of yttria stabilized zirconia (YSZ) coating. Ceram Int 2009;35:2493–7. https://doi.org/10.1016/j.ceramint.2008.11.012.

[20] Luo X, Yang Y, Yang Y, Tian D, Lu X, Chen Y, et al. Reduced-temperature redox-stable LSM as a novel symmetrical electrode material for SOFCs. Electrochim Acta 2018;260:121–8. https://doi.org/10.1016/j.electacta.2017.11.071.

[21] Darbandi AJ, Enz T, Hahn H. Synthesis and characterization of nanoparticulate films for intermediate temperature solid oxide fuel cells. Solid State Ionics 2009;180:424–30. https://doi.org/10.1016/j.ssi.2009.01.004.

[22] Jiang Y. Electrochemical reduction of oxygen on a strontium doped lanthanum manganite electrode. Solid State Ionics 1998;110:111–9. https://doi.org/10.1016/S0167-2738(98)00111-8.

[23] Haanappel VAC, Mertens J, Rutenbeck D, Tropartz C, Herzhof W, Sebold D, et al. Optimisation of processing and microstructural parameters of LSM cathodes to improve the electrochemical performance of anode-supported SOFCs. J Power Sources 2005;141:216–26. https://doi.org/10.1016/j.jpowsour.2004.09.016.

[24] Carpanese MP, Clematis D, Bertei A, Giuliano A, Sanson A, Mercadelli E, et al. Understanding the electrochemical behaviour of LSM-based SOFC cathodes. Part I — Experimental and electrochemical. Solid State Ionics 2017;301:106–15. https://doi.org/10.1016/j.ssi.2017.01.007.

[25] Bertei A, Carpanese MP, Clematis D, Barbucci A, Bazant MZ, Nicolella C. Understanding the electrochemical behaviour of LSM-based SOFC cathodes. Part II - Mechanistic modelling and physically-based interpretation. Solid State Ionics 2017;303:181–90. https://doi.org/10.1016/j.ssi.2016.09.028.

[26] Seyed-Vakili SV, Babaei A, Ataie M, Heshmati-Manesh S, Abdizadeh H. Enhanced performance of La0.8Sr0.2MnO3 cathode for solid oxide fuel cells by co-infiltration of metal and ceramic precursors. J Alloys Compd 2018;737:433–41. https://doi.org/10.1016/j.jallcom.2017.12.092.

[27] Tarragó DP, Malfatti C de F, de Sousa VC. Obtaining process of ceramic film on substrate by Airbrushed Solution Combustion (ASC) [BR 10 2017 008343 8 A2], 2017.

[28] Florio DZ de, Fonseca FC, Muccillo ENS, Muccillo R. Materiais cerâmicos para células a combustível. Cerâmica 2004;50:275–90. https://doi.org/10.1590/S0366-69132004000400002.

[29] YOKOKAWA H, SAKAI N, KAWADA T, DOKIYA M. Thermodynamic stabilities of perovskite oxides for electrodes and other electrochemical materials. Solid State Ionics 1992;52:43–56. https://doi.org/10.1016/0167-2738(92)90090-C.

[30] Chen RF, Huang Y, Wang CA. Characterization Methods of Pores in Ceramics and Their Analysis. Key Eng Mater 2007;280–283:1819–22. https://doi.org/10.4028/www.scientific.net/KEM.280-283.1819.

[31] Gerstl M, Navickas E, Leitgeb M, Friedbacher G, Kubel F, Fleig J. The grain and grain boundary impedance of sol–gel prepared thin layers of yttria stabilized zirconia (YSZ). Solid State Ionics 2012;225:732–6. https://doi.org/10.1016/j.ssi.2012.02.012.

[32] Gaudon M, Laberty-Robert C, Ansart F, Stevens P, Rousset A. Preparation and characterization of La1–xSrxMnO3+δ (0⩽x⩽0.6) powder by sol–gel processing. Solid State Sci 2002;4:125–33. https://doi.org/10.1016/S1293-2558(01)01208-0.

[33] Cortés-Gil R, Alonso JM, Ruiz-González ML, González-Calbet JM. Topotactic Migration of Cationic Vacancies in La1-tMn1-tO3. Eur J Inorg Chem 2010;2010:3436–40. https://doi.org/10.1002/ejic.201000086.

[34] Tarragó DP, Malfatti C de F, de Sousa VC. Influence of fuel on morphology of

LSM powders obtained by solution combustion synthesis. Powder Technol 2015;269:481–7. https://doi.org/10.1016/j.powtec.2014.09.037.

[35] BRANT M, MATENCIO T, DESSEMOND L, DOMINGUES R. Electrical degradation of porous and dense LSM/YSZ interface. Solid State Ionics 2006;177:915–21. https://doi.org/10.1016/j.ssi.2006.02.012.

[36] Niu Y, Lv W, Chen D, Han J, He W. A model study on correlation between microstructure-gas diffusion and Cr deposition in porous LSM/YSZ cathodes of solid oxide fuel cells. Int J Hydrogen Energy 2019;44:18319–29. https://doi.org/10.1016/j.ijhydene.2019.05.115.

[37] Su C, Lü Z, Wang C, Li J, Li P, Yue X, et al. Effects of a YSZ porous layer between electrolyte and oxygen electrode in solid oxide electrolysis cells on the electrochemical performance and stability. Int J Hydrogen Energy 2019;44:14493–9. https://doi.org/10.1016/j.ijhydene.2019.04.092.

[38] Abdelaziem A, El-Khatib KM, Hafez MA, Badr Y. Effect of annealing on La0.8Sr0.2MnO3 thin films prepared by pulsed laser deposition. Spectrochim Acta Part A Mol Biomol Spectrosc 2019;211:100–7. https://doi.org/10.1016/j.saa.2018.11.060.

[39] Chiba R, Vargas RA, Andreoli M, Seo ESM. Forming of Cathodic Ceramic Film Using Airbrush for Application in High Temperature Solid Oxide Fuel Cells. Mater Sci Forum 2012;727–728:669–74. https://doi.org/10.4028/www.scientific.net/MSF.727-728.669.

[40] Jiang S. A comparison of O2 reduction reactions on porous (La,Sr)MnO3 and (La,Sr)(Co,Fe)O3 electrodes. Solid State Ionics 2002;146:1–22. https://doi.org/10.1016/S0167-2738(01)00997-3.

[41] Das D, Basu RN. Improved polarization behaviour of nanostructured La0.65Sr0.3MnO3 cathode with engineered morphology. Int J Hydrogen Energy 2017;42:15347–58. https://doi.org/10.1016/j.ijhydene.2017.04.254.

[42] Benamira M, Ringuedé A, Cassir M, Horwat D, Pierson JF, Lenormand P, et al. Comparison Between Ultrathin Films of YSZ Deposited at the Solid Oxide Fuel Cell Cathode/Electrolyte Interface by Atomic Layer Deposition, Dip- Coating or Sputtering. Open Fuels Energy Sci J 2009;2:87–99. https://doi.org/10.2174/1876973X01002010087.

[43] Im J, Park I, Shin D. Preparation of nano-crystalline strontium-doped lanthanum manganate (LSM) powder and porous film by aerosol flame deposition. Ceram Int 2014;40:5567–73. https://doi.org/10.1016/j.ceramint.2013.10.148.

[44] Murray EP, Tsai T, Barnett SA. Oxygen transfer processes in (La,Sr)MnO3/Y2O3-stabilized ZrO2 cathodes: an impedance spectroscopy study. Solid State Ionics 1998;110:235–43. https://doi.org/10.1016/S0167-2738(98)00142-8.

[45] Andersson M, Yuan J, Sundn B. SOFC modeling considering electrochemical reactions at the active three phase boundaries. Int J Heat Mass Transf 2012;55:773–88. https://doi.org/10.1016/j.ijheatmasstransfer.2011.10.032.

[46] Ananyev MV, Farlenkov AS, Eremin VA, Kurumchin EK. Degradation kinetics of

LSM–YSZ cathode materials for SOFC. Int J Hydrogen Energy 2018;43:951–9. https://doi.org/10.1016/j.ijhydene.2017.11.107.

[47] Cole KS, Cole RH. Dispersion and Absorption in Dielectrics I. Alternating Current Characteristics. J Chem Phys 1941;9:341–51. https://doi.org/10.1063/1.1750906.

[48] Morales JCR, Vásquez JC, López DM, Martínez JP, Coll DP, Núñez P, et al. Caracterización electroquímica. Pilas Combust. óxidos solidos. 1ª ed., Tenerife: Centro de la Cultura Popular Canaria; 2008, p. 203–42.

[49] Barbucci A, Bozzo R, Cerisola G, Costamagna P. Characterisation of composite SOFC cathodes using electrochemical impedance spectroscopy. Analysis of Pt/YSZ and LSM/YSZ electrodes. Electrochim Acta 2002;47:2183–8. https://doi.org/10.1016/S0013-4686(02)00095-6.

[50] Tarragó DP, Moreno B, Chinarro E, Jurado JR, Malfatti C de F, de Sousa VC. Sintering and electrical properties of strontium- doped lanthanum manganite. Proc. 5th Int. Work. Hydrog. Fuel Cells, Campinas/SP - Brazil: 2010, p. 188–93.

[51] GHOSH A, SAHU A, GULNAR A, SURI A. Synthesis and characterization of lanthanum strontium manganite. Scr Mater 2005;52:1305–9. https://doi.org/10.1016/j.scriptamat.2005.02.020.

[52] Lee H. Electrochemical characteristics of La1−xSrxMnO3 for solid oxide fuel cell. Mater Chem Phys 2003;77:639–46. https://doi.org/10.1016/S0254-0584(02)00091-3.

[53] Yang J, Muroyama H, Matsui T, Eguchi K. A comparative study on polarization behavior of (La,Sr)MnO3 and (La,Sr)CoO3 cathodes for solid oxide fuel cells. Int J Hydrogen Energy 2010;35:10505–12. https://doi.org/10.1016/j.ijhydene.2010.07.174.

[54] Gleiter H. Nanostructured materials: basic concepts and microstructure. Acta Mater 2000;48:1–29. https://doi.org/10.1016/S1359-6454(99)00285-2.

[55] Fan L, Zhu B, Su P-C, He C. Nanomaterials and technologies for low temperature solid oxide fuel cells: Recent advances, challenges and opportunities. Nano Energy 2018;45:148–76. https://doi.org/10.1016/j.nanoen.2017.12.044.

[56] Meng B, Kong M, Yang QQ, Zhang H, Zhu YJ, Lin ZL. Effects of grain-boundary diffusions and modifications on the electrical conductivities of YSZ coatings with columnar microstructure. Solid State Ionics 2014;268:48–53. https://doi.org/10.1016/j.ssi.2014.09.024.

[57] KWON O, CHOI G. Electrical conductivity of thick film YSZ. Solid State Ionics 2006;177:3057–62. https://doi.org/10.1016/j.ssi.2006.07.039.

***Declaration of Interest Statement**

Declaration of interests

☒ The authors declare that they have no known competing financial interests or personal relationships that could have appeared to influence the work reported in this paper.

☐The authors declare the following financial interests/personal relationships which may be considered as potential competing interests: